February, 2006 Paris

Ultra-High Energy Cosmic Rays, Neutrinos and Gamma-Rays

D.V.Semikoz

APC, Collège de France,

11, pl. Marcelin Berthelot, Paris 75005, France

CONTENTS

1. INTRODUCTION:EXPERIMENTAL PUZZLES

1.1 Cosmic Rays

Cosmic Rays (CR) are radiation consisting of energetic particles originating beyond the Earth that impinge on the Earth's atmosphere. Cosmic rays are composed mainly of protons and heavier atomic nuclei. Electrons, gamma rays, and neutrinos also make up a smaller fraction of the cosmic radiation.

Flux of cosmic rays drops very fast with increasing of energy and can be approximated by power law $1/E^{2.7}$ over many orders of magnitude, see Fig. 1.1. At lower energies $E < 100$ TeV CR flux is still high enough to detect CR directly from space or by balloon experiments. Above 100 TeV s CR can produce showers in atmosphere which can be detected in the mountains.

Cosmic rays with energies $E > 10^{18}$ eV called Ultra High Energy Cosmic Rays (UHECR). They produce extensive air showers which can be detected practically at sea level or just within 1 km above it. Such showers consist from small fraction of high energy hadrons propagating along the direction of original UHECR particle (called shower axis) with typical spread of tens of meters around it and from large number of secondary low energy electrons, positrons, photons and muons, spread over the distances up to several kilometers from shower axis on the Earth surface. One can measure either the secondary particles by the net of detectors on ground or the fluorescence light emitted by the low energy electrons during their propagation in the atmosphere. These are two major technics used in the UHECR experiments.

In this chapter I will focus on results of two recent experiments. First, ground-

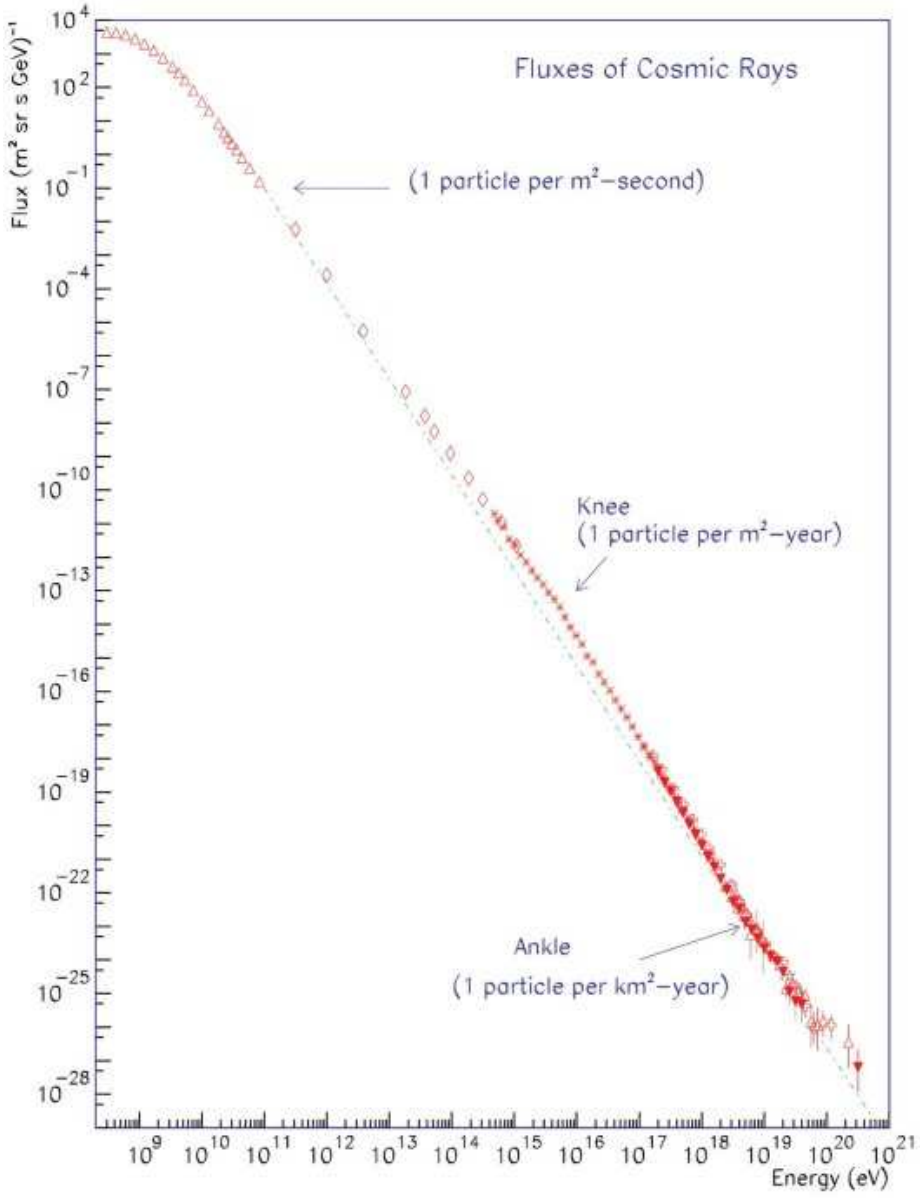

Fig. 1.1: Spectrum of cosmic rays at all energies from review ref. [9].

based AGASA [1] experiment consisted of 111 detectors which covered 100 km^2 area. It was located in Japan and operated in period 1993-2004. Second, fluorescent experiment HiRes [2], which consists from two telescopes, named HiRes I and HiRes II, located in Utah, USA and operated from 1999 till present time. In the following sections I will summarize experimental data on the UHECR energy spectrum, chemical composition of cosmic rays (i.e. fractions of protons, iron and photons in total UHECR flux), anisotropy signals in arrival directions and search for UHECR sources.

1.2 UHECR energy spectrum

UHECR experiments measure energy E of every event with typical errors $\Delta E/E \sim 25\%$, which allow to combine events in 10 independent energy bins per decade of energy. Figure 1.2a shows energy spectrum or differential flux of Akeno [3], AGASA [1] and HiRes [2] experiments. It is multiplied by E^3 in order to see details of steeply falling spectra.

Akeno experiment was dense array of detectors with total area of 1 km^2 and it measured UHECR flux in energy range 10^{15} eV $< E < 10^{18}$ eV. At low energies $E < 10^{17}$ eV amplitude of Akeno flux is completely consistent with many other experiments and we put Akeno data here for the purpose of absolute normalization at low energies.

The two HiRes telescopes are not equivalent. HiRes I operated longer and, due to this fact, collected larger data set then HiRes II at high energies. From other side HiRes II has two rows of mirrors, which allow it to significantly reduce energy threshold from $E > 4 \times 10^{18}$ for HiRes I to $E > 2 \times 10^{17}$ for HiRes II.

In order to combine the AGASA [1] with the Akeno [3] data in Fig. 1.2b, we have rescaled systematically the AGASA data 10% downwards in energy which is well within the uncertainty of the absolute energy scale of AGASA [1]. After that

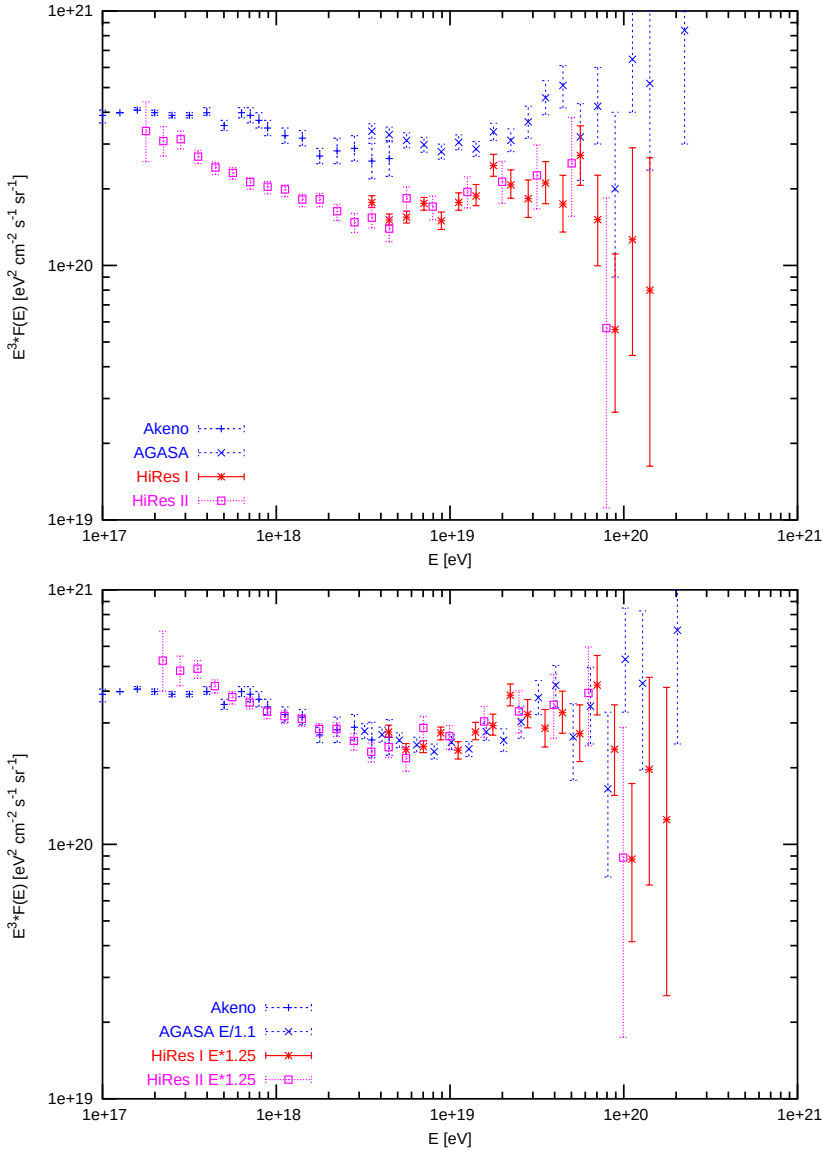

Fig. 1.2: a. Spectrum of UHECR measured by Akeno [3], AGASA [1] and HiRes [2] experiments. b. AGASA energy reduced by 10% and HiRes energy increased by 25% to Akeno energy scale.

there is still 25 % difference in energy scale between Akeno/AGASA and HiRes. In Fig. 1.2b we systematically scaled HiRes energies up to Akeno energy scale, however one can shift AGASA and high energy part of Akeno down in similar way or shift all spectra to some point in between.

The 25% difference in the energy scale between two technics is the first of existing puzzles in UHECR data. The question who is right, AGASA or HiRes would be answered within next year or two by new experiment Pierre Auger Observatory [4] which for the first time combine both technics.

The UHECR proton spectrum should be strongly suppressed above $E \gtrsim 5 \times 10^{19}$ eV due to pion production on cosmic microwave photons, the so called Greisen-Zatsepin-Kuzmin (GZK) cutoff [5]. Same is true for all nuclei due to their photodisintegration on infrared/optical background. As one can see from Fig. 1.2 the evidence for or against the presence of this cutoff in the experimental data is at present contradictory from data AGASA or HiRes. However this contradiction has significance 2.5-3 σ (this is significance of AGASA excess). Moreover AGASA excess can be an artifact due to unknown systematics. For example, in our paper [6] it was shown that atmospheric electric fields may affect the cosmic ray observations in several ways and may lead to an overestimation of the cosmic ray energies. The electric field in thunderclouds can be as high as a few kV/cm. This field can accelerate the shower electrons and can feed some additional energy into the shower. Therefore, ground array observations in certain weather conditions may overestimate by 20% the energy of ultra-high energy cosmic rays if they don't take this effect into account. In addition, the electric field can bend the muon trajectories and affect the direction and energy reconstruction of inclined showers. Finally, there is a possibility of an avalanche multiplication of the shower electrons due to a runaway breakdown, which may lead to a significant miscalculation of the cosmic ray energy [6].

At the moment question of existence of GZK cutoff is open, mainly due to very

small statistics (11 events in AGASA and 4 in HiRes). Auger experiment at $E > 10^{20}$ eV is 50 times more sensitive then AGASA and in AGASA-like case would be able to see 50 events per year. However first results published at ICRC 2005 [7] show that spectrum is rather suppressed based on limited statistics similar to one of AGASA. In HiRes-like case of spectrum Auger still can see ~ 10 events per year with $E > 10^{20}$ eV and in two years from now statistics would be large enough to resolve finally question of existence of GZK cutoff.

Besides existence of cutoff itself there is puzzle with events with $E > 10^{20}$ even in case of cutoff. They should come from nearby sources within 50 Mpc from Earth. Even in conservative case of renormalization of AGASA data to HiRes energy scale there are 5 events in AGASA data and 4 events in HiRes mono data with $E > 10^{20}$ plus famous Fly's Eye event with energy $E \approx 3 \times 10^{20}$ eV. So far searches of sources in direction of some of those cosmic rays did not give any hints [8]. This fact plus consistency of AGASA data with continuation of flux above GZK cutoff lead to wide discussion of top-down models, see for review [9] and some details in the related sections in this thesis.

Another feature in the UHECR spectrum in Fig. 1.2b is a dip (often called "ankle") in the around $4-8\times10^{18}$ eV seen in the experimental data both of AGASA and HiRes, as well as in older experiments like Yakutsk [10] or Fly's Eye [11]. Exact position of dip depends on systematic error in energy determination, discussed above. The fact that dip-ankle was seen in all relevant experiments make sure that this feature is a real effect.

There are two major explanations for ankle, which depend on chemical composition measurement. According to first of them ankle caused by transition between Galactic (heavy nuclei) and extragalactic (protons) components in UHECR spectrum [12]. According to second this dip may be caused by energy losses of protons due to e^+e^- pair production on cosmic microwave photons [13, 14] and was inter-

preted by the authors of Ref. [15] as signature for the dominance of extragalactic protons in the CR flux.

The UHECR spectrum in energy range 10^{17} eV $< E <$ 10^{19} eV would be investigated in details by Telescope Array experiment, which could be constructed in near future in Utah, USA [16]. Similarly to Auger Telescope Array experiment would combine both ground array and fluorescence detectors. This will allow it to choose between two explanations of ankle by study of UHECR chemical composition. We will discuss present status of the UHECR chemical composition searches in the next section.

1.3 Composition of UHECR

At any given energy UHECR flux consists from the fractions of protons, heavy nuclei, photons and neutrinos. The composition of UHECR at high energies is still unknown. In order to divide UHECR flux between different species one need in the independent observable which would be sensitive to chemical composition of primary particles.

Such observable for fluorescence detectors is depth of shower maximum $X_{\max}$, i.e. depth in atmosphere at which density of secondary particles is maximum. For example, for vertical shower with $E = 10^{19}$ eV maximum depth for iron nuclei would be around 700 g/cm^2, for protons it would be $750 - 800$ g/cm^2 and for photons 1000 g/cm^2, i.e. such photon showers would reach their maximum at ground level. Number of electrons in the shower development which define amount of fluorescent light and $X_{\max}$ slowly varies depending on assumed hadronic model for iron nuclei and photons. From other side for proton difference between model predictions for position of $X_{\max}$ at most reach 40 g/cm^2, which is still below difference between $X_{\max}$ for proton and iron. Of course, it is much easy to distinguish photons, for which showers develop much deeper in atmosphere. As was recently shown in ref. [17]

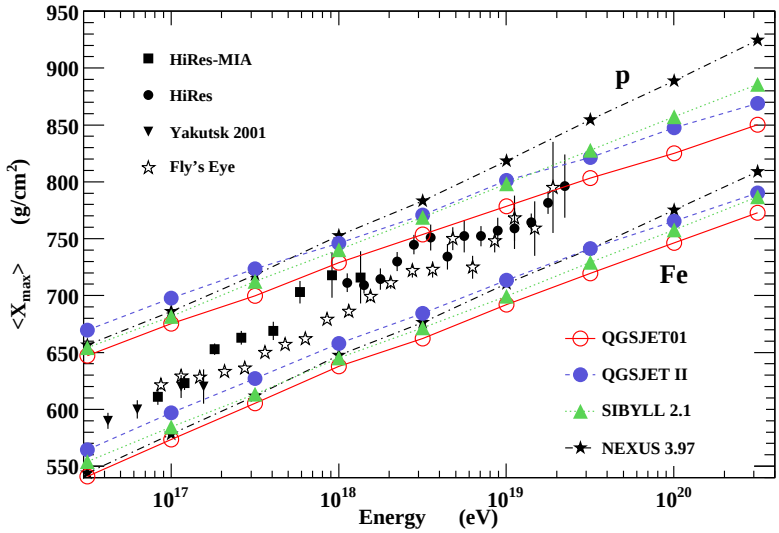

Fig. 1.3: Composition study from comparison of the shower maximum $X_{\max}$ measurement as function of energy with predictions of hadronic models from ref. [17].

all fluorescent data show that at 10^{17} eV spectrum dominated by iron, but around $E \sim 5 \times 10^{18}$ eV it is mostly proton dominated. However, details depend both on hadronic models used and also differ in transition region between HiRes-MiA and Fly's Eye data [17].

For ground array AGASA one can measure composition measuring both electromagnetic and muon components [18]. AGASA is consistent with 60% protons above 10^{19} eV, but result is more strongly model dependent because muon component predictions in hadronic models can differ by 30% to be compared to few percent difference in the electromagnetic component, which affects fluorescence detector predictions.

The analysis of the muon content in air showers has been used by AGASA to reject photon dominance in UHECR above 10^{19} eV [18]. Assuming a composition of protons plus photons, AGASA quotes upper limits for the photon ratio of 34%, 59% and 63% at 10^{19} eV, $10^{19.25}$ eV and $10^{19.5}$ eV respectively at the 95% confidence

level [18]. Also a reanalysis of horizontal showers at Haverah Park concluded that photons cannot constitute more that 50% of the UHECR above 4×10^{19} eV [19].

At highest energies, 6 events in AGASA data with $E > 10^{20}$ eV allow to put limit to photon fraction at level of 50-65% [20, 21], which can be reduced to 36% by adding 4 more events from Yakutsk data [21]. Those limits strongly restrict some theoretical models which predict high photon flux at $E > 10^{20}$ eV in order to explain AGASA data above GZK cutoff. At 10^{19} eV the best limit comes from Pierre Auger Observatory, with results that photon flux above this energy does not exceed 26 % [22]. This limit will be definitely improved in near future, which will also allow to restrict some exotic models which predict high photon flux. We will discuss those restrictions in more details in Section 2.5.5.

1.4 Anisotropy in arrival directions

For every event together with energy cosmic ray experiments define arrival directions. In general UHECR data are isotropic at all energies, which in case of charge primaries is expected due to large deflections in magnetic fields. However, at highest energies $E > 10^{19}$ eV one can expect in case of small extragalactic magnetic fields (see discussion on magnetic fields in next chapter) that UHECR protons from nearby sources would show up excess in some directions, which possibly allows in future to find sources of cosmic rays. Let me also note here that all searches of anisotropy at very large scales, like correlations with galactic or extragalactic plane did not show any significant correlations at high energies $E > 10^{19}$ eV. In the contrary at even higher energies $E > 10^{20}$ eV there are some hints of anisotropy at scales of few degrees (usually called small scales) and on moderate scales of 15 -30 degrees, which we will discuss in the following sections.

1.4.1 Small scale clusters

The AGASA data on the arrival direction of cosmic rays with energies $E > 4\times10^{19}$ eV are in general isotopically distributed. However it contain a clustered component with 4 pairs and one triplet within 2.5 degrees [23, 24]. 57 AGASA events with energies $E > 4 \times 10^{19}$ eV are presented by crosses in Fig. 1.4 in Equatorial coordinates.

The authors of Ref. [25] used first the angular two-point auto-correlation function w discussing the significance of small-scale clustering in the arrival directions of UHECRs. Since the signal of point-like sources should be concentrated around zero angular distance $\delta_{ij} = 0$, one can restrict analysis to the value of w in the first bin,

$$w_1 = \sum_{i=1}^{N} \sum_{j=1}^{i-1} \Theta(\delta_1 - \delta_{ij}) \,, \tag{1.1}$$

where δ_{ij} is the angular distance between the two cosmic rays i and j, δ_1 the chosen bin size, Θ the step function, and N the number of CRs considered.

Exact value of probability that "clustering signal is by chance" depends both on energy cutoff $E_{\rm cut}$ in the data and on bin size δ_1. One can increase signal-to-noise ratio scanning over one or both those parameters, but one needs to calculate penalty factor for making such scan. In Ref. [25] Tinyakov and Tkachev suggested that angular scale $\delta_1 = 2.5^\circ$ is related to AGASA angular distribution, following original AGASA claim [23, 24]. In this case for all 57 AGASA events probability to see signal by chance is $P_{\rm chance}(57) \sim 10^{-3}$. They also made scan over energy cutoff and found that best fit point correspond to 36 highest energy events and probability decreased by order of magnitude $P_{\rm chance}(36) \sim 10^{-4}$. However, one needs to take into account penalty for this scanning procedure [26], which gives factor 3 in above example and final probability is $P_{\rm chance} \sim 3 \times 10^{-4}$ factor 3 smaller then one for total dataset.

A draw-back of using only the first bin of the autocorrelation function w is the dependence of the results on δ_1. As a possible solution, one can perform a scan over different bin sizes and calculate the resulting penalty factor both for energy and

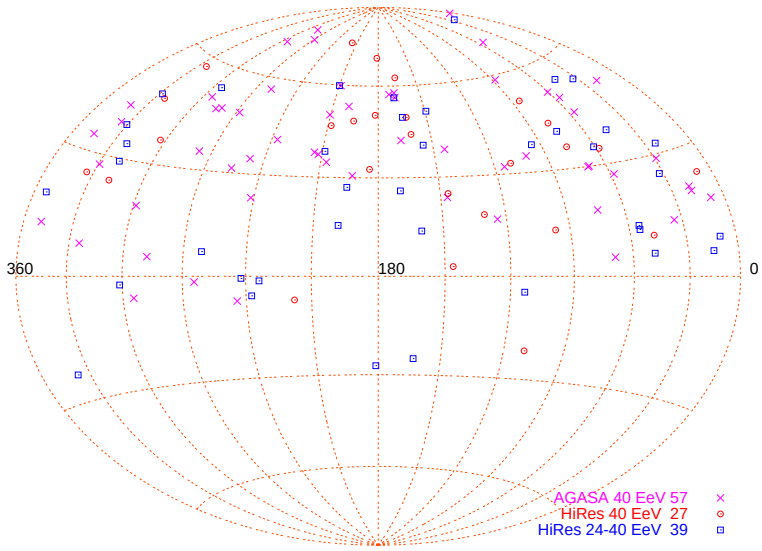

Fig. 1.4: Sky map of highest energy AGASA and HiRes data.

angle [27]. However, the result then still depends on the minimal and maximal bin size used in the scan: Choosing the scan range too large reduces the signal-to-noise ratio and thus diminishes the signal, while a too small range overestimates the signal. Final conclusion of ref. [27] was that $P_{\rm chance}(AGASA) \sim 3 \times 10^{-3}$.

Of course, the ultimate test of observed AGASA signal would be to check it with new independent data. HiRes monocular data from HiRes I or HiRes II are not suitable for this purpose because they precisely define only direction perpendicular to shower plane, and along plane resolution is as bad as 10-20 degrees. However, events observed by two detectors together (stereo events) are resolved with precision up to 0.5 degree. Thus HiRes stereo data can serve as test for AGASA clustering signal.

In Fig. 1.4 we presented sky map of arrival directions of 57 AGASA events with $E > 4 \times 10^{19}$ eV, 27 HiRes events with $E > 4 \times 10^{19}$ eV and 39 HiRes events with 2.4×10^{19} eV $< E < 4 \times 10^{19}$ eV. Already at this map one can see that there is no single doublet along 27 highest energy HiRes events with any small angular separation.

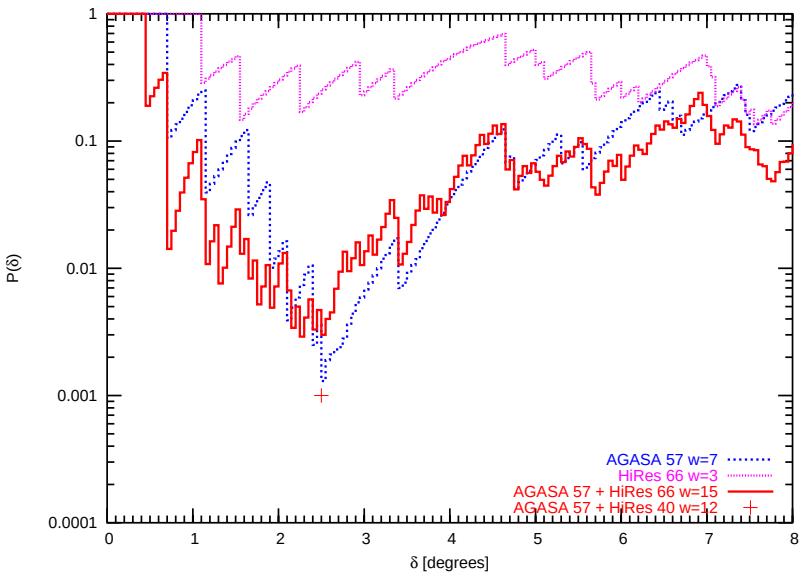

Fig. 1.5: Probability that small scale clustering signal seen by chance as function of angle for AGASA with $E > 4 \times 10^{19}$ eV (57 events), HiRes stereo data with $E > 2.4 \times 10^{19}$ eV (66 events) and combined data set (123 events). The cross shows probability for the combined data set of AGASA and 40 HiRes events with $E > 3 \times 10^{19}$ eV.

Unfortunately, exact arrival directions of HiRes data with energy $E > 3 \times 10^{19}$ eV are not public (this energy corresponds to AGASA energy $E > 4 \times 10^{19}$ eV after shift by 35 % in Fig. 1.2). Instead we present here bigger public data set with $E > 2.4 \times 10^{19}$ eV.

As one can see from Fig. 1.2, due to shift between AGASA and HiRes data, one should shift energy threshold by 30 - 35% before comparing them. HiRes collaboration shows that after such shift they have 40 events with $E > 3 \times 10^{19}$ eV with only one doublet, which is compatible with background [28]. In Fig. 1.2 we plot probability of clustering for 66 HiRes events with $E > 2.4 \times 10^{19}$ eV and public arrival directions with magenta line. One can see that clustering signal is not significant at any small angle, even there are 3 doublets within 2.5 degrees angular scale.

The conclusion of HiRes collaboration was they can not confirm AGASA signal. However separate question is does this negative result means that AGASA saw fake fluctuation? Already in [29] it was shown that both results do not contradict each other even if signal in AGASA is real. Later in paper ref. [30] HiRes collaboration shows that one of their events with energy $E \sim 3.7 \times 10^{19}$ eV is falling exactly to the position of AGASA triplet (see Fig. 1.4). Probability that such quadruplet is by chance is $P \sim 4 \times 10^{-3}$. It was estimated by likelihood method.

Autocorrelation analysis of combined data set was never done. For 40 HiRes events with $E > 3 \times 10^{19}$ eV and value for autocorrelation function at angular scale 2.5 degrees is $w = 12$ [31], which allows us to calculate probability for combined 57 AGASA + 40 HiRes events scaled to AGASA energy scale $E > 4 \times 10^{19}$ as $P \sim 10^{-3}$. This probability is presented with the cross in Fig. 1.5.

We also calculated probability for combination of 66 HiRes events with public arrival directions and 57 AGASA events, shown with red line in Fig. 1.5. One can see that strength of the signal of combined data set is as strong as one for AGASA along. Unfortunately, I can not do two-dimensional analysis here including energy threshold, because energies of individual HiRes events are not public. However, present analysis

show that combines AGASA - HiRes data, properly shifted to same energy scale shows autocorrelation signal at the level of $P \sim 10^{-3}$.

Thus, we conclude that even if AGASA small scale clustering signal was not confirmed by HiRes data along, combined dataset show a signal as significant as AGASA one. If signal is real, then AGASA saw fluctuation up and HiRes fluctuation down in it. Of course, clustering signal is dominated by combined 4-plet, and it is unclear, either one sees single source on sky, or one starts to see point-like sources. Answer on this question would be done within one year from now by Auger collaboration.

1.4.2 Clustering on moderate scales

In our recent paper ref. [32] we (M. Kachelriess and myself) for the first time looked on arrival directions in UHECR data at moderate scales 10-30 degrees. In this section I will briefly discuss results of this analysis.

In order to make combine analysis one needs first to renormalize data of all experiments to same energy scale, as discussed in previous section [32]. In Fig. 1.6, one can see a sky map in equatorial coordinates of the arrival directions of the UHECR used in the analysis, number of events and energy cut of each data set shown in figure caption. An inspection by eye indicates several overdense regions like one around and south the AGASA triplet as well as several underdense regions or voids.

In same way as for small scale clustering signal, one can calculate two point correlation function and comparing to Monte Carlo random data sets find the chance probability $P(\delta)$, that observed clustering signal at given angles is by chance. In Fig. 1.7, we show the chance probability $P(\delta)$ as function of the angular scale δ for different combinations of experimental data. The chance probability $P(\delta)$ shows already a 2σ minimum around 20–30 degrees using only the 27 events of the HiRes experiments with $E' \geq 4 \times 10^{19}$ eV. Adding more data, the signal around $\delta = 25^{\circ}$ becomes stronger, increasing from $\sim 2\sigma$ for 27 events to $\sim 3.5\sigma$ for 107 events. It

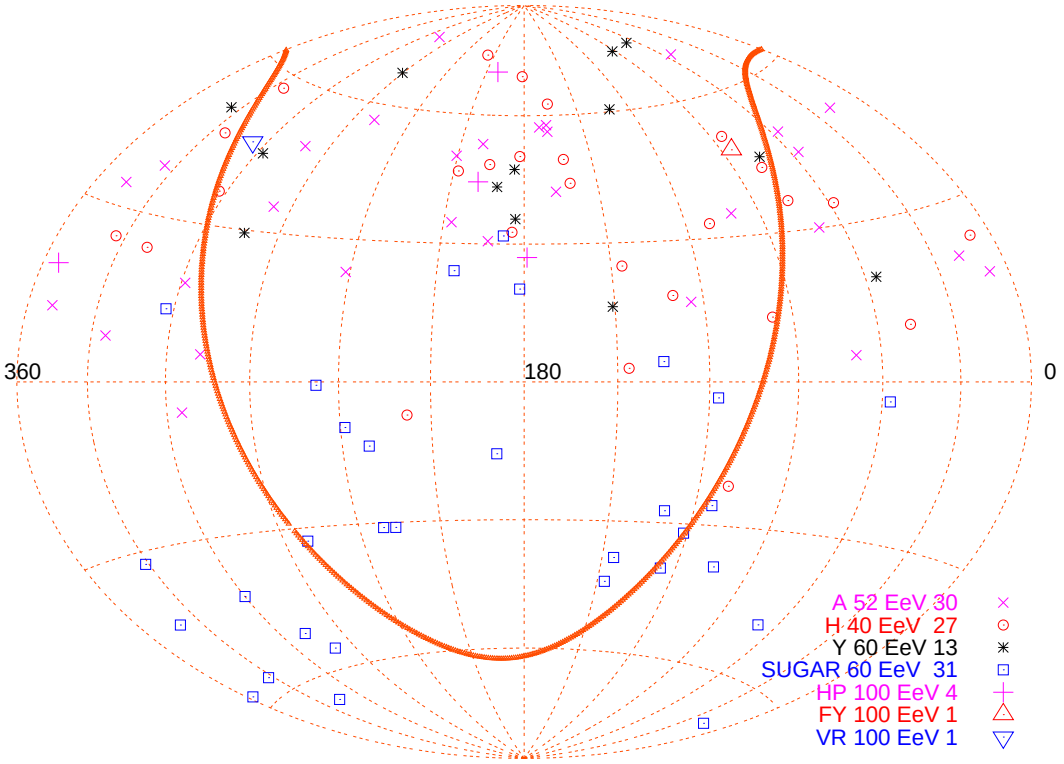

Fig. 1.6: Sky map of the UHECR arrival directions of events with rescaled energy $E' > 4 \times 10^{19}$ eV in equatorial coordinates; magenta crosses–30 AGASA (A) events with $E > 5.2 \times 10^{19}$ eV, red circles–27 HiRes (H) events with $E > 4 \times 10^{19}$ eV, black stars–13 Yakutsk (Y) events with $E > 6 \times 10^{19}$ eV, blue boxes–31 Sugar (S) events with $E > 6 \times 10^{19}$ eV, magenta crosses–4 Haverah Park (HP) events with $E > 10^{20}$ eV, red triangle–one Fly's Eye (FY) event with $E > 10^{20}$ eV, blue triangle–Volcano Ranch (VR) event with $E > 10^{20}$ eV.

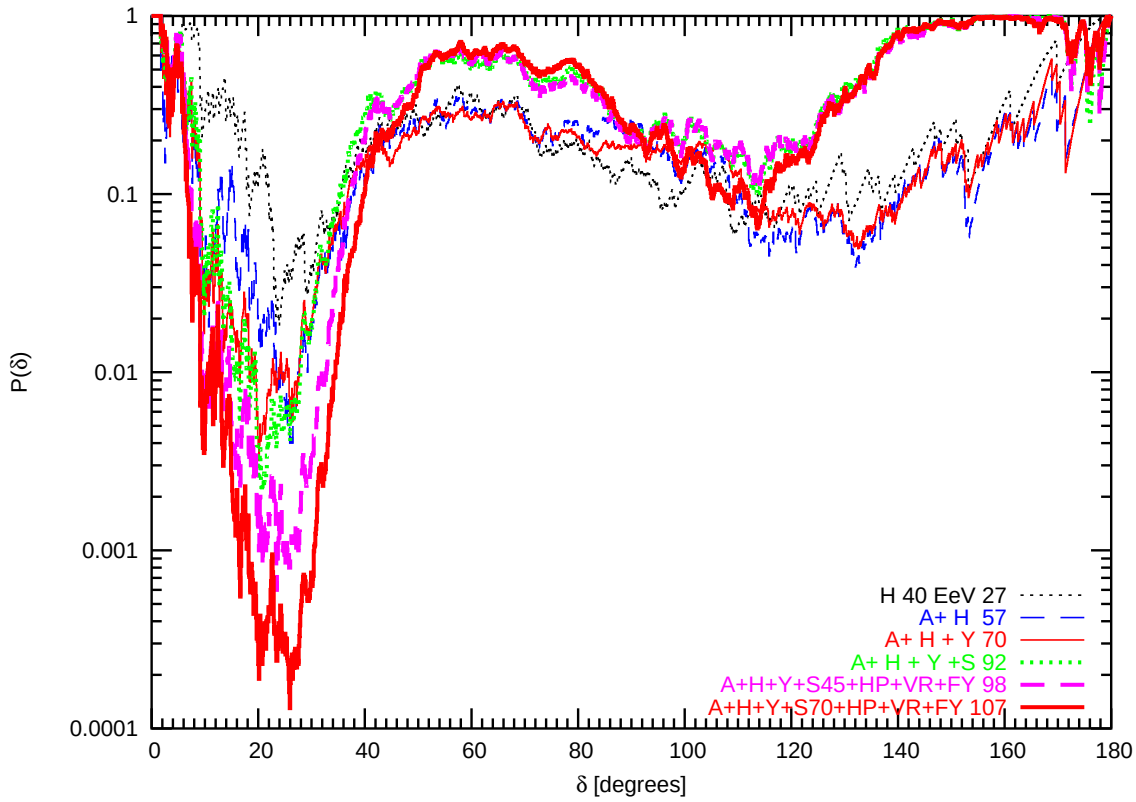

Fig. 1.7: Chance probability $P(\delta)$ to observe a larger value of the autocorrelation function as function of the angular scale δ for different combinations of experimental data; label of experiments as in Fig. 1.6.

is comforting that the position of the minimum of $P(\delta)$ is quite stable adding more data and every additional experimental data set contributes to the signal. Moreover, autocorrelations at scales smaller than 25° become more significant increasing the data set. However, we warn the reader again that we have not constrained ourselves a priori to search for autocorrelations at $\delta = 20°$ and hence the numerical values of the chance probability found should not be taken at face value. In particular, penalty factor for not searching signal at 20° *a priori* is around 30 (see details in ref. [32]). Thus probability to have such signal by chance is $P_{\rm chance} \sim 3 \times 10^{-3}$.

Above results, if confirmed by future independent data sets, have several important consequences.

Firstly, anisotropies on intermediate angular scales constrain the chemical composition of UHECRs. Iron nuclei propagate in the Galactic magnetic field in a quasi-diffusive regime at $E = 4 \times 10^{19}$ eV (i.e. does not have ballistic trajectories but can not be confined for long in Galaxy) and all correlations would be smeared out on scales as small as observed by us. Therefore, models with a dominating extragalactic iron component at the highest energies are disfavored by anisotropies on intermediate angular scales.

Secondly, the probability that small-scale clusters are indeed from point sources will be reduced if the clusters are in regions with an higher UHECR flux. For example, the AGASA triplet is located in an over-dense spot (cf. map in Fig. 1.6) and the probability to see a cluster in this region by chance is increased. In contrast, the observation of clusters in the "voids" of Fig. 1.6 would be less likely by chance than in the case of an UHECR flux without medium scale anisotropies.

However, the most important consequence of our findings is the prediction that astronomy with UHECRs is possible at the highest energies. The minimal energy required seems to be around $E' = 4 \times 10^{19}$ eV, because low energy data arrive more and more isotopically [32]. This trend is expected, because at lower energies both

deflections in magnetic fields and the average distance l from which UHECRs can arrive increase. Since the two-dimensional sky map corresponds to averaging all three-dimensional structures (with typical scale L) over the distance l, no anisotropies are expected for $l \gg L$. Thus, if the signal found in this analysis around 20-30 degrees is confirmed it will have to be related to the local large scale structure.

Finally, we note that Ref. [33] found that around 400 events are needed to reject the hypothesis that the UHECR sources trace the galaxy distribution. We consider it as an fluctuation that the HiRes data set alone (as well as the SUGAR data set with zenith angle $\theta = 70^\circ$) shows already a 2σ signal with 27 events. To check this signal, an independent data set of order $O(100)$ events with $E' > 4 \times 10^{19}$ eV is required.

1.5 Search for UHECR sources

Anisotropy signals, discussed in previous section can give hints for searches of UHECR sources. However for moderate scales connection between UHECR sources and observed signal can be non-trivially connected with modeling of magnetic fields. From other side clustering signal on small scales can be used for positional search of sources in directions of clusters, assuming that events in given cluster come from the same source.

This argument allowed Tinyakov and Tkachev to find correlations of AGASA data with $E > 4 \times 10^{20}$eV with BL Lacertae objects or BL Lacs [34]. They chose brightest BL Lacs from catalog with magnitude $mag < 18$. Under this cut there are 156 BL Lacs in catalog, some of which correlate with AGASA cosmic rays. Namely 11 from 57 AGASA cosmic rays correlate with 9 BL Lac objects from catalog within 2.5 degrees with probability by chance $P \sim 2 \times 10^{-2}$ (this signal strongly improves with the assumption that UHECR are protons deflected in galactic magnetic field $P \sim 10^{-4}$ [35]).

This signal can be improved either by making additional cuts in catalog of BL Lacs either directly [34] or by cross-correlations with catalog of EGRET sources [36]. However both subsets of BL Lacs which maximize AGASA signal, did not show any significant correlations with the HiRes data [37].

Another independent signal was found recently in correlations of HiRes data with $E > 10^{19}$ eV with same 156 BL Lac objects with angular separation compatible to HiRes angular resolution [38]. Namely, within 0.8 degrees from 156 BL Lac objects there are 11 cosmic rays (from 271), while for random data set only 3 expected. Probability that this signal by chance is $P \sim 4 \times 10^{-4}$. The most interesting and important consequence of this result is that only neutral particles can explain correlations with such small angular separation. From other side both photons and neutrons can not reach Earth from distant BL Lacs. Thus such signal, if confirmed in future can be explained only by new physics!

In recent paper ref. [37] HiRes collaboration investigated in details correlations of their data with different subclasses of blazars. They found that what besides BL Lacs their data with $E > 10^{19}$ eV correlate with 47 HP blazars with $mag < 18$ with probability that correlation is by chance $P \sim 6 \times 10^{-3}$, as well as with 5 established TeV blazars (which are subset of BL Lacs and HP blazars) with probability that correlation is by chance $P \sim 10^{-3}$. HiRes collaboration plans to check above correlations with independent data set of new data.

In ref. [39] it was calculated how many data one needs to collect in new experiments like Auger and Telescope Array in order to check correlations, found by HiRes. Besides HiRes itself, which plan to publish their data in few months, Auger will be able to check above claims within less then one year from now, according to numbers in ref. [39].

Finally, in ref. [40] all existing claims of different source correlations was reanalyzed together with conclusion, that only significant correlations seen so far was correlations

with BL Lacertae objects.

To summarize, BL Lacertae (and HP blazars) are promising sources at least of part of UHECRs. If HiRes and Auger confirm correlations with those distant sources with small angles, one will need new physics to explain such correlations. For today, this is the strongest signal in UHECR data which requires existence of new physics.

In the following chapter UHECR data will be discussed within the framework of the Standard Model of the Elementary Particles. And in the final chapter we will review several exotic models, in particular those, which explain AGASA spectrum above GZK cutoff, and those which explain correlations of UHECR data with BL Lacertae objects by the existance of new neutral particles.

2. PROTONS AS UHECR. SECONDARY NEUTRINOS AND PHOTONS.

As was discussed in Introduction, UHECR chemical composition studies suggest that at energies $E > 10^{19}$ eV protons dominate in UHECR spectrum. Because protons of those energies can not be randomized by the Galactic magnetic field, and UHECR arrival directions are isotropic on large angular scales, those protons should come from extragalactic sources. In this chapter we will assume that major part of UHECR above $E > 10^{19}$ eV are protons and secondaries of their interaction with the Cosmic Microwave Background Radiation (CMBR) and other soft photon backgrounds. Also in case of HiRes experiment [41] chemical composition is proton dominated already from $E > 10^{18}$ eV, and we will try to explain its spectrum with protons starting from this energy. In the following sections we will discuss possible proton acceleration mechanisms, their interactions in the intergalactic medium and production of secondary photons and neutrinos.

2.1 Acceleration. Sources of UHECR protons. Secondary gamma-rays and neutrinos from sources.

Charged particles can be accelerated in astrophysical objects either by shock waves due to Fermi mechanism of the first order, or by electric fields which can exist is those objects. Maximum energy to which protons can be accelerated without taking into account energy losses is [42]:

$$E_{\max} = eZRB \ , \tag{2.1}$$

where eZ is the particle charge, R is the size of the acceleration region and B is the typical magnetic field. Already this simple estimate suggested by Hillas in 1985 allows to restrict possible astrophysical accelerators at highest energies $E \sim 10^{20}$ eV [42].

However, if one takes into account possible energy losses due to the synchrotron radiation or interactions with medium in the source acceleration to such high energy becomes very challenging problem for existing acceleration models. Most popular models discuss proton acceleration by first order Fermi mechanism (see, for example, Refs.[43, 44]). Here I will not discuss advantages and disadvantages of such models of proton acceleration. Instead in the following sections I will describe alternative model of proton acceleration by electric field in the AGN core [45, 46], formation of AGN jets in this model [47] and production of secondary neutrinos [48].

2.1.1 Proton acceleration by black hole in AGN core

It is known that particles can be accelerated near the horizon of a black hole of a mass $M = M_9 \times 10^9 M_\odot$ to energies $E_{max} \sim 3 \times 10^{20} B_3 M_9$ eV ($B = B_3 \times 10^3$ G is magnetic field strength) [49]. In the first approximation we can suppose that in the direct vicinity of the horizon (inside the last stable orbit, where there is no accretion disk) the magnetic field is ordered on the scale of $R_g = 2GM$ and is directed along the black hole rotation axis. In this case the rotational drag of inertial coordinate frames near the black hole horizon leads to generation of electric field with quadrupole geometry [50], see Fig. 2.1.

An important feature of the resulting electromagnetic field configuration is that electric field $\vec{E}$ is aligned with magnetic field $\vec{B}$ in the regions around the black hole rotation axis. Charged particles accelerated by this electric field are ejected into two collimated oppositely directed beams along the axis. This mechanism was suggested for acceleration of proton to ultra-high energies in our paper with A. Neronov [45].

The opening angle of the beam can be estimated if we note that the particle

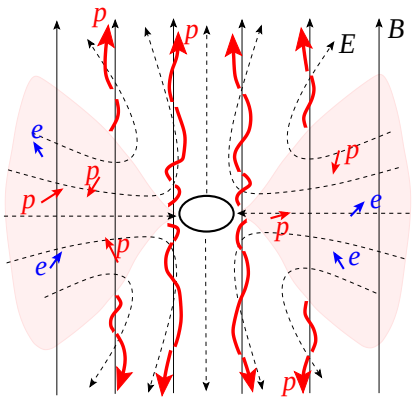

Fig. 2.1: Rotating black hole placed into a homogeneous magnetic field. The electric field induced by the rotation is shown by dashed lines. Particles with high initial latitudes are accelerated along the magnetic field lines and ejected into two oppositely directed collimated beams along the rotation axis. Particles of low latitudes are confined in the shaded regions around equatorial plane [45].

motion is a superposition of the motion along z axis with the speed $v_z \approx c$ and the drift in the orthogonal direction with the speed $v_\perp = E_\perp/B$ [51]. Using the explicit expression for electro-magnetic field near horizon [50] we find that the opening angle of the beam of particles ejected from initial distance $R_0 \geq 3GM$ is $\theta \leq v_\perp/c \approx 1.1^o a/M$ ($a = J/M \leq M$ is the black hole rotation moment).

Recent more detailed studies of this model [46] confirm that protons can be accelerated by such mechanism up to $E = 3 \times 10^{20}$ eV taking into account energy losses in acceleration process. However a large amount of high energy photons in GeV-TeV range of energies are coproduced during such acceleration.

Depending on value of the photon background around the black hole, accelerated protons either can escape from AGN core or interact with the soft photon backgrounds surrounding black hole and produce secondaries pions which decay on UHE photons and neutrinos. Also this process can be dynamical in time and the same object can

produce both UHECR protons, photons and neutrinos at different times with time scales vary from months to thousands of years.

Considered model provides a simple explanation for the origin of nonthermal VHE electrons in large and small scale jets and enables to relate directly radio-to-X-ray data on the AGN jets to the physical processes in the vicinity of the black hole horizon. In next subsection I will briefly discuss possible large scale jet model within such scenario.

2.1.2 AGN jets powered by UHE photons.

The radiative cooling of electrons responsible for the nonthermal synchrotron emission of large scale jets of radio galaxies and quasars requires quasi continuous (in time and space) production of relativistic electrons throughout the jets over the scales exceeding 100 kpc. While in the standard paradigm of large scale jets this implies *in situ* acceleration of electrons, in our paper Ref. [47] it was proposed a principally different "non-acceleration" origin of these electrons, assuming that they are implemented all over the length of the jet through effective development of electromagnetic cascades initiated by extremely high energy γ-rays injected into the jet from the central object.

The electromagnetic cascade initiated by very high energy (VHE) photons interacting with ambient radiation fields in the large scale extragalactic jets is an attractive mechanism for production of ultra-relativistic electrons (with almost 100 percent efficiency) which can be responsible for the observed radio-to-X-ray spectra of jets, see Fig. 2.2. The trajectories of electrons with energies below $E_{\rm crit} \sim 10$ TeV are isotropized by the random magnetic field B_r [47]. Such electrons form a "shell" around the cascade. Observer, who looks at the jet from a side, sees synchrotron and inverse Compton radiation only form the "shell" electrons. The cascade can be developed effectively in the jet provided that the strength of the random B-field does not exceed 1 μG. On the other hand, when at a very large distances from the central

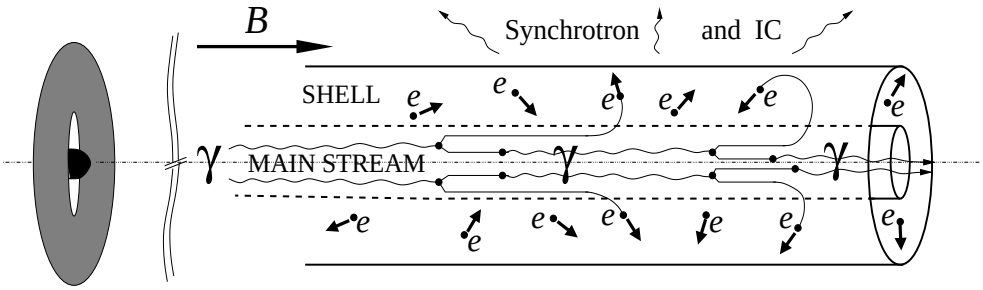

Fig. 2.2: Extremely high energy gamma-rays, $E \gg 10^{16}$ eV, from central engine form the "main stream" of the jet and provide high energy electrons throughout the entire jet. The low energy electrons below the critical energy $E_{\rm crit}$ escape the "main stream" and form a "shell" of the jet. Distant observer see the synchrotron and inverse Compton radiation from electrons in the "shell".

source the random field is reduced to a very low level comparable with the intergalactic field, $B \sim 10^{-9}$ eV or less, the cascade continues almost rectilinearly until the 10-100 TeV γ-rays start to interact effectively with the diffuse infrared background photons. This interaction would lead to the formation of *observable* giant pair halos with specific angular and energy distributions depending on the intensity of diffuse infrared background at the cosmological epoch corresponding to the redshift of the central source z [52]. And finally, if the central source is a blazar, i.e. the jet is pointed to the observer, we may expect beamed γ-ray emission with a characteristic for cascades $E^{-1.5}$ type spectrum extending to 100 TeV. However, due to significant intergalactic absorption, the γ-rays will arrive with significantly distorted spectra.

The protons accelerated by a black hole in the model discussed in Section 2.1.1 can produce VHE γ-rays interacting with the ambient photon fields (supplied, for example by accretion disk around the massive black hole) through photo-meson process. For hot accreation disk $T \sim 10^4$K VHE photons with $E > 10^{17}$ eV can still escape from production area [47]. In same process VHE neutrinos are coproduced with VHE photons from decays of charge pions. We will discuss those neutrinos in the next

section.

2.1.3 Neutrinos from GeV-loud blazars

In this section we will discuss possible sources of very high energy neutrinos, following our ref. [48]. The main idea how one can estimate an upper limit on neutrino flux from given source is in connection between neutrino flux and the high energy photon flux, under assumption that photon flux was caused by the same pion production process in the interaction of accelerated protons with medium in the source.

The Universe is not transparent for photons with energies above 100 GeV due to pair production on background photons: $\gamma + \gamma_B \to e^+ + e^-$. The highest energy photons from astrophysical objects (nearby TeV blazars) seen so far had energies $E \sim 10^{13}$ eV. No direct information about emission of $E > 10^{13}$ eV photons is available now. At the same time it is well established that photon emission from blazars (active galactic nuclei (AGN), with jets, which we see almost face on) in the MeV-TeV energy range is highly anisotropic. Typical estimates of the γ factors of the emitting plasma, $\gamma \sim 10$, imply that in the 10^{6-13} eV band almost all γ-ray flux is radiated in a cone with the opening angle $\theta \sim 1/\gamma \sim 5^\circ$. Particles (photons, neutrinos) in the higher energy range $E > 10^{13}$ eV can be emitted in an even narrower cone. This fact favors blazars as promising neutrino sources.

An estimate of the neutrino flux from sources can be obtained from the detected γ-ray flux. The GeV γ-rays can be produced in the AGN core through a variety of mechanisms: inverse Compton scattering of electrons on soft background photons, synchrotron radiation of very-high energy protons in magnetic fields, development of electromagnetic cascade initiated by photo-pion production. Neutrinos can be produced only in the last case. However, it is important to note that the γ-ray flux from a given source can be even lower than the neutrino flux. Electromagnetic cascade on background photons in source spread photon flux over large angle (up to $4\,\pi$) while

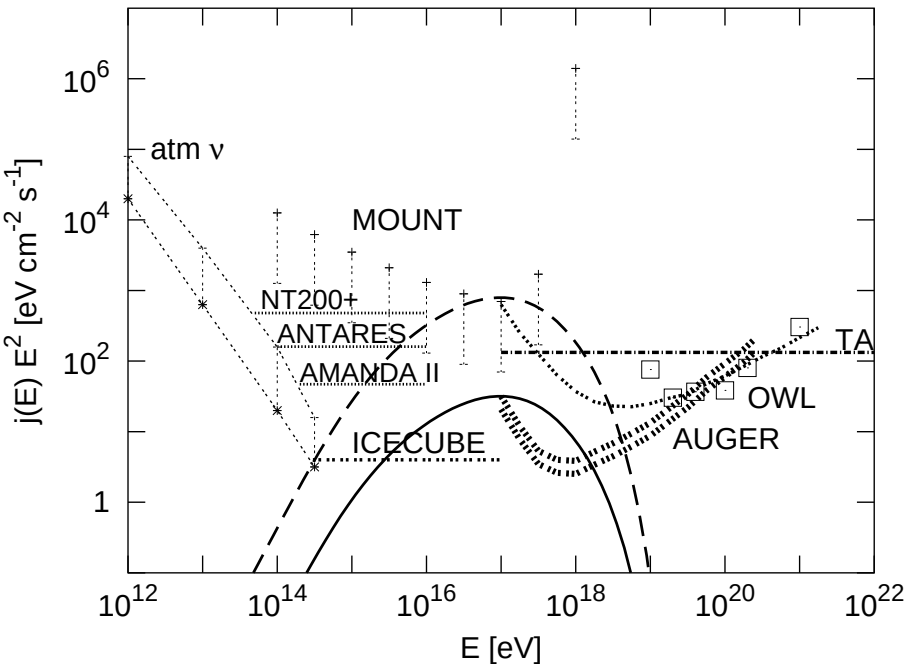

Fig. 2.3: Neutrino flux from typical GeV-loud EGRET blazar (thick solid line) compared with expected sensitivities to electron/muon and tau-neutrinos in detectors AMANDA II [54], Auger [55], and the planned projects: Telescope Array (TA) [56] (dashed-dotted line), the fluorescence/Čerenkov detector MOUNT [57], the space based OWL/EUSO [58, 59] (indicated by squares), the water-based Baikal (NT200+) [60], ANTARES [61] (the NESTOR [62] sensitivity would be similar to ANTARES according to Ref. [63]), and the ice-based ICECUBE [64], as indicated. All not published experimental sensitivities are scaled from corresponding diffuse sensitivities with the same factor as ICECUBE. The dashed line is for an opening angle for neutrino 5 times smaller than the opening angle for GeV photons.

neutrinos practically does not interact in the source and their flux stay collimated in direction of original jet [48].

In ref. [48] we suggested GeV-load EGRET blazars [53] as possible candidates for neutrino sources. In Fig. 2.3 we present possible neutrino flux from typical GeV-loud EGRET blazar in two cases: when the neutrino flux is similar to photon flux, and when neutrino flux is collimated in small angle (1 degree instead of 5 degree for GeV photons). In first case only ICECUBE and may be Pierre Auger Observatory after long term operation will be able to detect neutrino fluxes from point-like sources. In the last case many other experiments will be able to see the neutrino flux from the sources discussed in ref. [48]. However, the smaller opening angle for neutrino flux will reduce the number of neutrino sources. Let us note here, that the ANITA radio experiment [65, 66], which will be most sensitive to diffuse neutrino flux, will not be able to compete in point source searches, presented in Fig. 2.3, because it can see only small fraction of sky near Earth equator [66].

2.1.4 Neutrinos from TeV blazars

In ref. [48] we also explained why neutrinos can not be produced in TeV-blazars in interactions of UHE protons with background photon fields. Let us make a simplest estimate of the optical depth in the direction from the center of the core toward the Earth for TeV-blazars. The fact that TeV γ-rays produced in the vicinity of the central black hole are able to escape from the core and reach the Earth means that the mean free path of TeV photons with respect to pair production on background photons,

$$R_\gamma = \frac{1}{\sigma_{\gamma\gamma} n_{\rm soft}} \ , \tag{2.2}$$

($\sigma_{\gamma\gamma} \sim \sigma_T = 6.6 \times 10^{-25}$ cm^2 is the cross-section of pair production for center-of-mass energies close to the pair production threshold; $n_{\rm soft}$ is the angle-dependent number

density of the soft photons) is larger than the core size in the direction toward the Earth

$$R_\gamma > R_{\rm core}. \tag{2.3}$$

The cross-section $\sigma_{p\gamma} \sim 10^{-28}$ cm^2 of interactions of protons with the same soft photons is more than three orders of magnitude smaller than $\sigma_{\gamma\gamma}$. Thus, the mean free path for protons must be at least

$$R_p \geq 10^3 R_{\rm core} \ , \tag{2.4}$$

which means that just a negligible fraction of protons propagating in the direction of the interest interacts with the soft photons in the core.

The situation would be very different if protons interact with matter background. In this case the hadronic cross section larger than the electromagnetic one

$$\sigma_{pA} > \sigma_{\gamma\gamma} \tag{2.5}$$

and one can produce neutrinos and TeV photons at the same time. Interesting that there is a hint of possible neutrino signal in AMANDA-II detector from TeV source 1ES 1959+650 [67]. Two neutrino events from direction to this source arrive at the same time as so called orphan TeV gamma-ray flares (i.e. when TeV gamma-ray flare is not accompanied by flare in X-rays). It is difficult to estimate probability for such coincidence because AMANDA analysis was done *a posteriori*, however formal probability for such coincidence without penalty factors is 10^{-3}. One really needs more data to confirm or reject this hint.

It is also interesting that the same TeV source is one of those which contribute to the neutral correlations of HiRes UHECR data with $E > 10^{19}$ eV with TeV blazars. Namely arrival direction of one of the HiRes UHECR events coincides with 1ES 1959+650 within 0.5 degree, i.e. within angular resolution of this experiment [68]. Because proton of such energy expected to be deflected at least in Galactic magnetic

field on larger angle, expected events should be neutral particles. Neutrons with $E = 10^{19}$ eV would decay on the way from source after 1 Mpc. UHECR photons can reach us from those objects only under unrealistically extreme conditions, like acceleration of protons up to $E = 10^{23}$eV [69]. Thus, if such correlations would be confirmed in future by Auger data, it would require existance of new physics.

Of course, both AMANDA neutrino signal and HiRes UHECR data need in confirmation. In any case, if neutrinos are produced in TeV sources like Mkn421, Mkn 501 or 1ES 1959+650, the production mechanism should be through $p + A$ interactions rather then through $p + \gamma$. Because TeV sources remain good candidates for acceleration of protons to ultra-high energy. However accelerated protons still can lose their energy on the way from distant sources to the Earth. We will discuss their propagation in the next section.

2.2 Propagation of protons.

Once escaped from sources protons still have to reach Earth. One the way they can be deflected both by extragalactic and Galactic magnetic fields and can lose energy in interactions with photon backgrounds and due to redshifting.

Let us first discuss energy losses. The relevant processes are redshift due to universe expansion, electron-positron pair production by protons ($p\gamma_b \to pe^-e^+$), photoproduction of single pion $N\gamma_b \to \Delta \to N'\pi$ or multiple pions ($N\gamma_b \to N\ n\pi$, $n \gg 1$) and neutron decay. Pion production processes described in detail in ref. [70], while pair production by proton in ref. [71]. Related distances on which protons will lose energy in "e" times, which are presented in Fig. 2.4 calculated with our numerical code of ref. [72]. This propagation code was tested by detailed comparison on the level of individual reactions with older code ref. [70] and show good agreement.

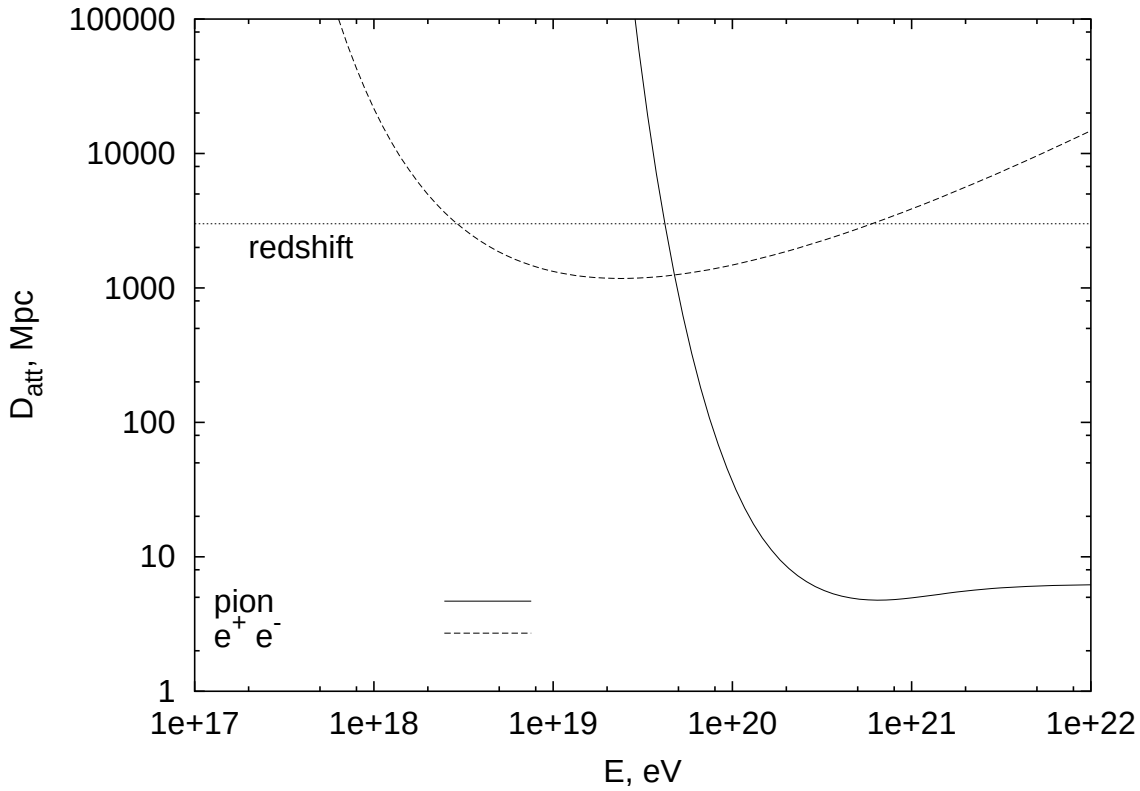

Fig. 2.4: Proton attenuation length as function of energy for three main energy losses: pion production, $e^{\pm}$ pair production and redshift of Universe. Calculated with code of ref. [72].

Single pion production is possible for proton energies above threshold:

$$E_{th} = \frac{m_\pi^2 + 2M_P m_\pi}{4\epsilon_0} \approx 4 \times 10^{19} \text{ eV} , \tag{2.6}$$

where m_π and M_P are pion and proton masses and $\epsilon_0 = \pi^4 T_0/30\zeta(3) \approx 6.4 \times 10^{-4}$ eV is average energy of CMBR background.

At energies above E_{th} in Eq. (2.6) single and multiple pion production on CMBR would dominate over other processes the rough estimate of energy loss distance for single pion production is:

$$L_{\text{pion}} = \frac{1}{K_\pi \sigma_{p\gamma} n_{\text{CMBR}}} \sim 10 \text{ Mpc} \tag{2.7}$$

where $K_\pi \approx m_\pi/M_P \approx 0.2$ is the proton energy loss in single pion production, $\sigma_{p\gamma} = 5 \times 10^{-28}$ cm^2 is photopion cross section and $n_{\rm CMBR} = 400/cm^3$ is CMBR photon density. For multi-pion production cross section is five times smaller but energy loss in the single interaction is almost 50 %.

Below this energy but above 3×10^{18} eV pair production by protons would dominate:

$$L_{e^+e^-} = \frac{1}{K_{e^+e^-}\sigma_{p\gamma\to pe^+e^-}n_{\rm CMBR}} \sim 1000 \text{ Mpc} , \tag{2.8}$$

where $K_{e^+e^-} \approx 2m_e/M_P \approx 10^{-3}$ is proton energy loss in pair production and pair production cross section is $\sigma_{p\gamma\to pe^+e^-} \sim \alpha^3/m_e^2 \sim 6 \times 10^{-28}$ cm^2.

At lower energies the most important process is redshifting, see Fig. 2.4.

Note that in Fig. 2.4 only interactions with CMBR are taken into account. In real calculations pion production on infrared/optical photons can be important for $E < 4 \times 10^{19}$ eV. The number of those photons is several hundred times lower than CMBR, $0.5 - 1/cm^3$, but their energy is higher then that of the CMBR. This will allow pion production at $E < 4 \times 10^{19}$ eV and this process will compete with pair production and redshift.

Different models of UHECR generation can be discriminated if sources are identified and distances to them are known. Unfortunately, the identification of particular sources is lost in the overall spectrum and one has to construct the observed spectra of individual sources as a function of the distance. This procedure was first carried out in Ref. [14], however, the wealth of information arising with this treatment may be represented in compact form in the way suggested in our paper [69]. First we construct individual spectra as a function of z. For each given spectra we find the value of energy at which the number of particles per decade of energy becomes smaller than the freely propagated particle flux by a given factor (3, 10, etc.). We thus plot energy obtained as a function of z. Results are presented in Fig. 2.5. We see that curves with

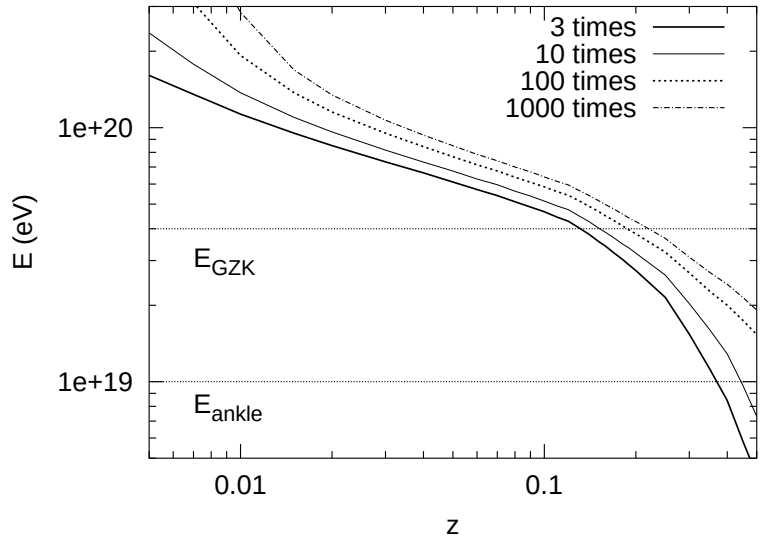

Fig. 2.5: Levels of a constant damping of the proton flux as a function of distance traversed.

an increasing damping factor converge rapidly in the range $0.01 \lesssim z \lesssim 0.5$, therefore, if the redshift to the source is in this range, Fig. 2.5 allows to determine maximal proton energies expected from this source.

The horizontal line at $E = E_{\rm GZK} \equiv 4{\times}10^{19}$ eV corresponds to the formal beginning of the GZK cut-off. Attenuation length at this energy is $l_a \sim 10^3$ Mpc. This may give a false impression that protons with $E = E_{\rm GZK}$ reach us from the sources located at $l = l_a$. Contribution of these protons is negligible as can be seen from Fig. 2.5: for $z > 0.2$ bulk of the protons have $E < 4 \times 10^{19}$ eV.

Besides energy losses propagation of protons is affected by deflections in Galactic and extragalactic magnetic fields. If the correlation length l_c of the ExtraGalactic Magnetic Field (EGMF) is much smaller than distance to the proton source d, then protons will diffuse in domains of EGMF. The average value of the proton deflection

in diffuse regime is:

$$\delta = 0.2^\circ \left(\frac{B}{10^{-10}G}\right)\left(\frac{10^{20}eV}{E}\right)\left(\frac{d}{100\ \mathrm{Mpc}}\right)^{1/2}\left(\frac{l_c}{1\ \mathrm{Mpc}}\right)^{1/2} \tag{2.9}$$

In the past average EGMF was assumed to be $B_{\mathrm{EG}} \sim 10^{-9}$ G everywhere in space, which is very rough approximation, because magnetic field is much larger in galaxy clusters and much smaller in the voids. Recently big progress was done in the calculation of tree-dimensional structure of extragalactic magnetic fields followed large scale structure simulations. Instead of average value $B_{\mathrm{EG}} \sim 10^{-9}$ G, new simulations allow to estimate cumulative filling factor for EGMF strength bigger then given value and as result fraction of cosmic rays which would be deflected on angles larger then given value. Results of two independent groups (refs. [73, 74]) show that magnetic fields with such values fill only part of the sky. However results of the two groups are very different in details. In ref. [73] magnetic fields with $B_{\mathrm{EG}} > 10^{-9}$ G fill 15 % of volume and $B_{\mathrm{EG}} < 10^{-11}$ G only in the 30% of the volume. In the contrary, in ref. [74] magnetic fields with $B_{\mathrm{EG}} > 10^{-9}$ G fill 0.02 % of volume and $B_{\mathrm{EG}} < 10^{-11}$ G the 95% of the volume. Such different results lead to contradictory results for deflections. For ref. [74] deflections are bigger then 1 degree only in one percent of the volume for cosmic rays with $E = 4 \times 10^{19}$ eV for distances up to 100 Mpc, assuming sources are outside of reach clusters. For ref. [73] deflections are as large as $\delta = 61^\circ$ for cosmic rays with $E = 4 \times 10^{19}$ eV for distances up to 100 Mpc, but for sources located within clusters. Let us note that recent independent calculation of ref. [75] suggest that $B_{\mathrm{EG}} > 10^{-9}$ G fill 1 % of volume and for $E > 10^{20}$eV cosmic rays deflected less then 0.2 degree in 99% of cases, which is more close to result of ref. [74]. Even if situation is not completely clear at the moment, in the following we will assume that extragalactic magnetic fields do not deflect cosmic rays on more then few degrees, because otherwise observed spectrum of cosmic rays can be significantly different from those of homogeneous distribution of sources, and have different connection to injection

spectrum at sources.

Finally let us briefly discuss deflections in Galactic magnetic field. It consist of coherent component with μG field mostly located in galactic disk and random component, of the same order in magnitude, but incoherent on kpc scales. Due to this fact contribution of random component to deflection of cosmic rays usually order of magnitude smaller as compared to deflection by regular component [76]. As for regular component, deflections strongly depends on model used. Recently, in ref. [77] three models, existing in literature [78, 79, 80] were compared in details. In general, deflections in Galactic magnetic field can be parameterize as following [77]:

$$\delta \approx 0.53^{\circ} Z \left(\frac{10^{20}\mathrm{eV}}{E}\right) \frac{B}{\mu G} \frac{L}{kpc} \ , \tag{2.10}$$

where Z is the particle charge, E its energy, B the effective value of magnetic field along trajectory and L the total pass through Galaxy. In general all models agree in order of magnitude deflections Eq. (2.10), which are for protons 1-2 degrees at $E = 10^{20}$ eV and 10-30 degrees at $E = 10^{19}$ eV. But in different regions of sky models predict deflections at different levels and sometimes even in opposite deflections. From other side, deflection in Galactic field are small enough to not prevent to search for UHECR sources at least at highest energies, $E > 4 \times 10^{19}$ eV.

Let us conclude that unless extragalactic magnetic fields are extremely large, i.e. even in some cases of relatively moderate deflections of ref. [73], spectrum of protons would not be affected by deflections in magnetic fields and can be investigated taking into account energy loss only. Additionally, in case of relatively small extragalactic magnetic files like in ref. [74] on can try to find sources of cosmic rays from their arrival directions. Contrary, for heavy nuclei already deflections in Galactic magnetic field would make search for sources from arrival directions very problematic [77]. In the next section we will discuss how density of UHECR sources can be found from the clustering signal observed in the cosmic ray arrival directions.

2.3 Density of UHECR sources

In this section we estimate the density of UHECR sources assuming that the clustered component observed by AGASA experiment is due to point-like sources. In many works small scale clustering signal was used to estimate parameters like the density n_s of sources or the strength of magnetic fields [81, 82, 83, 84, 85, 86]. The authors of Ref. [81] pointed out, for the first time, that the observation of small-scale clusters allows to determine the number density of CR sources. In practice, the observed small-scale clusters of AGASA were used to estimate the number CR sources first in the pioneering work of Dubovsky, Tinyakov and Tkachev [82].

In this section we will follow the presentation of our recent paper [87], where we made detailed Monte Carlo study of connection between small scale clustering signal and density of UHECR sources. We generated sources with constant comoving density n_s up to the maximal redshift $z = 0.2$. The flux of sources further away is negligible above 4×10^{19} eV, see Fig. 2.5. To any source i with equatorial coordinates Right Ascension R.A. and declination δ at comoving radial distance R_i we gave weight according to the declination dependent exposure [88] of the experiment and reduction of flux

$$g_i = \frac{1 + z_{\rm min}}{1 + z_i} \left(\frac{R_{\rm min}}{R_i} \right)^2 . \tag{2.11}$$

Here, $R_{\rm min}$ and $z_{\rm min}$ are the distance and redshift of the nearest source in the sample, respectively, and we have assumed the same luminosity for all sources. Then CRs are generated according to the injection spectrum $dN/dE \propto E^{-\alpha}$, where we fix $\alpha = 2.7$ to reproduce the AGASA energy spectrum below the GZK cutoff. We propagate CRs taking into account all energy losses discussed in Section 2.2 until their energy is below $E_{\rm min} = 4 \times 10^{19}$ eV or they reach the Earth. We also take into account the energy-dependent angular deflection through the Galactic magnetic field and the angular resolution of the experiments.

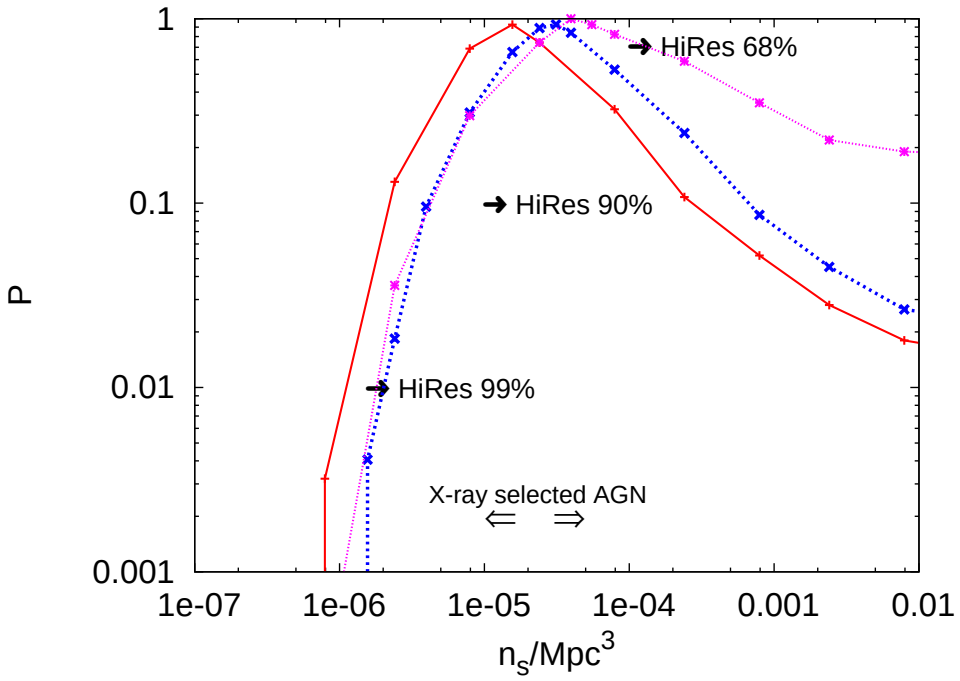

Fig. 2.6: Probability P that an uniform source distribution is consistent with number of clusters observed in the AGASA data as function of the density of sources n_s, with $N = 57$ (solid line) and $N = 72$ (dotted line) events for $\ell_1 = 2.5°$, and with $N = 57$ (dashed line) for $\ell_1 = 5°$. Lower limits on n_s from the HiRes stereo data (arrows) and the density range of X-ray selected AGNs with X-ray luminosity $L > 10^{43}$ erg/s are also shown.

One can In Fig. 2.6, the probability P that given density of sources consistent with the AGASA clustering signal as function of source density n_s for three different cases: The publicly available AGASA data set until May 2000 [89] ($N = 57$ or $E_{\rm min} = 4{\times}10^{19}$ eV) for the two bin sizes $\ell_1 = 2.5°$ ($w_1^* = 7$) and $\ell_1 = 5°$ ($w_1^* = 10$), and the complete AGASA data set [90] ($N = 72$ or $E_{\rm min} = 4 \times 10^{19}$ eV, bin size $\ell_1 = 2.5°$ and $w_1^* = 8$). Remarkably, the most likely value for the source density, $n_s = (1–4) \times 10^{-5}$/Mpc^3 is stable against an increase of the data set and a change in bin size. A similar value for $n_s \sim 10^{-5}$ was found previously by the authors of Ref. [86], while

earlier analyses [82, 83] using only events above $E = 10^{20}$ eV obtained larger values for n_s. The steep decrease of P for low n_s excludes already now uniformly distributed sources with much lower density than $10^{-6}/\mathrm{Mpc}^3$. For comparison, it is shown also the estimated density of powerful AGNs with X-ray luminosity $L > 10^{43}$ erg/s in the energy range 0.2–5 keV, $n_s \sim (1-5) \times 10^{-5}/\mathrm{Mpc}^3$ [91]. The density of Seyfert galaxies is about a factor of 20 higher. Note that most often only very specific subsets of AGNs with much lower densities are discussed as sources of UHECRs. On the other side, $P(w_1^*|\theta)$ decreases only slowly for large n_s. With the present AGASA data set it is therefore difficult to exclude large source densities.

Contrary to AGASA, HiRes stereo set with $N = 27$ events above 4×10^{19} eV contains no doublet within $\ell_1 = 2.5^\circ$ and 5° [92]. Thus HiRes data alone are consistent with a continuous source distribution. But since the number of events is small and P is a broad distribution, the HiRes data are also consistent with the best-fit value for n_s from the AGASA data, at 53% and 21% C.L. for $\ell_1 = 2.5^\circ$ and 5°, respectively. In Fig. 2.6, we show also lower limits on n_s for $\ell_1 = 5^\circ$ from the HiRes stereo data. Similar conclusions were obtained independently in Ref. [29]. Note that clustering signal for combined AGASA and Hires dataset, presented in Introduction, would not be very different from $N = 72$ AGASA data case in Fig. 2.6.

The effect of extragalactic magnetic fields on the above results is negligible, if the deflection is 2° on 500 Mpc propagation distance as found for a large part of the sky in Ref. [74]. The assumption of equal luminosity of all sources gives a lower bound on the possible number of sources [82]. A large additional population of faint sources cannot be excluded, if their contribution to the UHECR flux is sufficiently small. However, it is unlikely that any large population of sources can accelerate CRs to energies $\gtrsim 10^{19}$ eV.

We conclude that clustering signal in AGASA data, assuming that UHECR are protons and extragalactic magnetic field is small suggest that density of UHECR

sources is similar to density powerful AGNs. HiRes stereo data, if combined with AGASA as was described in the Introduction would give similar result. However, for definite statistical conclusion on source density on need in much larger data set, which will be provided by Pierre Auger Observatory after several years of observations.

In next section we will discuss how model of astrophysical sources emitting UHECR protons can explain UHECR spectrum for all energies $E > 10^{18}$ eV.

2.4 Minimal model of UHECR

In this section, we assume that UHECRs with $E \gtrsim 10^{18}$ eV are dominated by extragalactic protons as suggested by HiRes data [41]. Also we assume that GZK cutoff in cosmic ray spectrum exists. Next, we fix the density of sources with small scale clustering signal, as discussed in Section 2.3. We will ignore in this section HiRes - BL Lac correlations at $E \sim 10^{19}$ eV, which anyway give contribution only up to 3% to observed UHECR flux [38]. The goal is to describe UHECR energy spectrum with maximum realistic model of proton sources, which at the same time has minimal number of parameters. We will follow results of our recent paper [93].

It is usually assumed that the spectrum of an individual UHECR source has the form:

$$F(E) = 1/E^{\alpha} \;\; \theta(E_{\max} - E) \tag{2.12}$$

where α is spectrum index and $E_{\max}$ is the maximum energy to which source can accelerate protons.

Several groups of authors have tried previously to explain the observed spectral shape of UHECR flux using mainly two different approaches: In the first one, the ankle is identified with the transition from a steep galactic, usually iron-dominated component, to extragalactic protons with injection spectrum with $\alpha = 2 - 2.2$ in Eq.(2.12) as predicted by shock acceleration mechanism [94, 95, 96, 97, 98, 99]. In

the second approach, the dip is a feature of e^+e^- pair production and one is able to fit the UHECR spectrum down to $E \sim 10^{18}$ eV using only extragalactic protons and an injection spectrum with $\alpha = 2.6 - 2.7$ [15, 100, 101, 102]. The first possibility is not very predictive, because it assumes by construction that ankle is at the place where it is, fitting only the highest energy part of spectrum with $E > 10^{19}$ eV. In the second one an explanation for the complex spectrum suggested ad-hoc by the authors of Ref. [15] is missing. Moreover, an injection spectrum with $\alpha \approx 2.7$ is considerably steeper than $\alpha \approx 2$ predicted by shock acceleration [103].

A basic ingredient of all these analyses is the assumption that the sources are identical. In particular, it is assumed that every source can accelerate protons to the same maximal energy $E_{\rm max}$ in Eq. (2.12), typically chosen as 10^{21} eV or higher. However, one expects that $E_{\rm max}$ differs among the sources and that the number of potential sources becomes smaller and smaller for larger $E_{\rm max}$. Therefore two natural questions to ask are i) can one explain the observed CR spectrum with non-identical sources? And ii), is in this case a good fit of the CR spectrum possible with $\alpha \sim 2$ as predicted by Fermi shock acceleration?

In ref. [93] we proposed to use more realistic source models for the calculation of the energy spectrum expected from extragalactic protons. We relaxed the assumption of identical sources and suggested to use a power-law distribution for the maximal energies of the individual sources,

$$\frac{dn}{dE_{\rm max}} \propto E_{\rm max}^{-\beta} \,. \tag{2.13}$$

Without concrete models for the sources of UHECRs, one can not derive the exact form of the distribution of $E_{\rm max}$ values. However, the use of a power-law for the $E_{\rm max}$ distribution is strongly motivated by the following two reasons: First, we expect a monotonically decreasing distribution of $E_{\rm max}$ values and, for the limited range of two energy decades that we consider, a power-law distribution can be a good

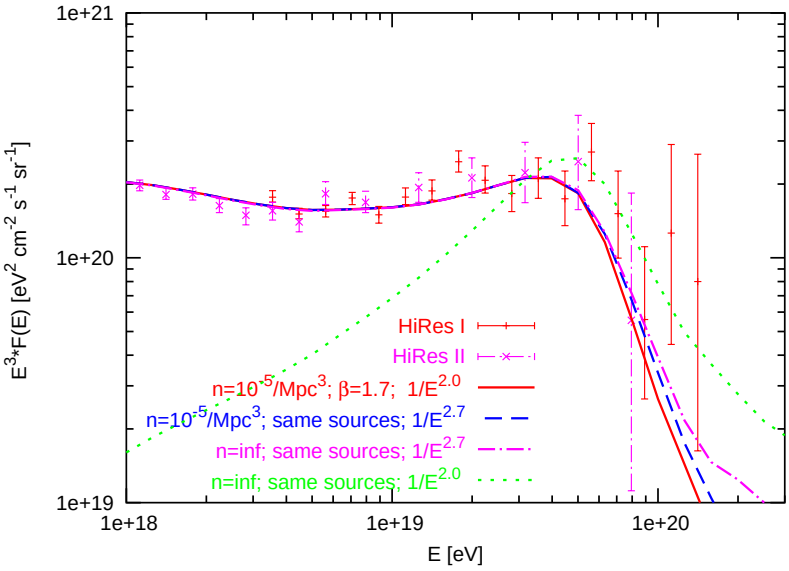

Fig. 2.7: Fits of the HiRes I and HiRes II data are shown for a uniform distribution of identical sources with power-law injection spectrum $1/E^2$ (green, dashed line) and $1/E^{2.7}$ (magenta, dash-dotted line) for an infinite number of sources as well as for a realistic source density $n_s = 10^{-5}/\mathrm{Mpc}^3$ and spectrum $1/E^{2.7}$ (blue, dashed line). The case of an $1/E^2$ spectrum and maximal energy dependence from Eq. (2.13) with $\beta = 1.7$ is shown as a red, solid line.

approximation to reality. Second, the use of a power-law distribution for E_{max} with exponent

$$\beta = \alpha_0 + 1 - \alpha\,, \tag{2.14}$$

guarantees to recover the spectra calculated with Eq. (2.12), i.e. $E_{\mathrm{max}} = \text{const.}$, for the special case of $E_{\mathrm{max}} \to \infty$ and a continuous distribution of sources. In Eq. (2.14), α denotes the exponent of the injection spectrum of an individual source and α_0 the exponent of the effective injection spectrum after averaging over the E_{max} distribution of individual sources. For instance, an injection spectrum of single sources with $\alpha = 2$ characteristic for Fermi shock acceleration reproduces effectively together with a distribution of E_{max} values with $\beta = 1.7$ the case $\alpha_0 = 2.7$ found assuming identical

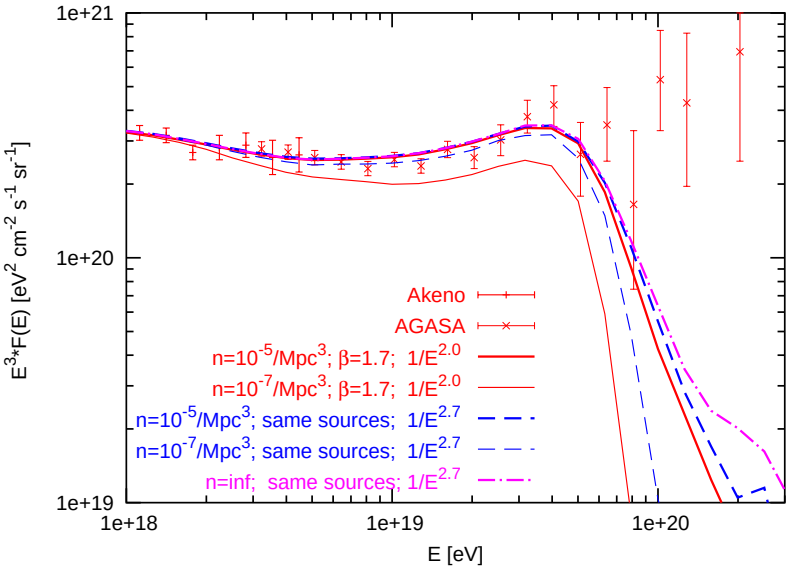

Fig. 2.8: The fit of Akeno/AGASA data using a uniform distribution of identical sources for an infinite number of sources and power-law spectrum $1/E^{2.7}$ is shown as a magenta, dash-dotted line. The same fit with the realistic source density $n_s = 10^{-5}/\mathrm{Mpc}^3$ and spectrum $1/E^{2.7}$ (thick blue dashed line) and $1/E^2$ spectrum and maximal energy dependence from Eq. (2.13) with $\beta = 1.7$ is shown as a thick red, solid line. The thin red, solid line for the spectrum $1/E^2$ and $\beta = 1.7$ and the thin blue, dashed line for the spectrum $1/E^{2.7}$ correspond to the low source density $n_s = 10^{-7}/\mathrm{Mpc}^3$.

sources. For finite values of $E_{\max}$ and the source density n_s, the effective injection spectrum is not described anymore by a single power-law. However, deviations show-up only at energies above $\approx 6 \times 10^{19}$ eV or small source densities, see below.

The results of our simulation are presented in Fig. 2.7 for HiRes and in Fig. 2.8 for Akeno/AGASA. In the standard picture of uniform sources with identical maximal energy (here, $E_{\max} = 10^{21}$ eV) and $1/E^2$ spectrum, extragalactic sources contribute only to a few bins of the spectrum around the GZK cutoff, cf. the green-dotted line in Fig. 2.7. By contrast, an injection spectrum $1/E^{2.7}$ allows one to explains the observed data down to $\approx 10^{18}$ eV with extragalactic protons from identical sources,

cf. the magenta, dash-dotted line for a continuous and the blue, dashed line for a finite source distribution with $n_s = 10^{-5}/\mathrm{Mpc}^3$ in Fig. 2.7. This well-known result can be obtained also for an injection spectrum $1/E^2$ of individual sources, if for the $E_{\max}$ distribution, Eq. (2.13), the exponent $\beta = 1.7$ is chosen. This is illustrated by the red, solid line in Fig. 2.7 for the case of a finite source density $n_s = 10^{-5}/\mathrm{Mpc}^3$. As already announced, only small differences at the highest energies, $E \gtrsim 6 \times 10^{19}$ eV, are visible between an effective $\alpha_0 = 2.7$ produced by an suitable $E_{\max}$ distribution and the case of identical sources with $\alpha = 2.7$ for large enough n_s.

In Fig. 2.8, we show the dependence of our results on the source density n_s together with the Akeno/AGASA data. While for large enough source densities, $n_s = 10^{-5}/\mathrm{Mpc}^3$, the spectra from identical sources with $1/E^{2.7}$ and from sources with $1/E^2$ injection spectrum, variable $E_{\max}$ and $\beta = 1.7$ are very similar, for smaller densities, $n = 10^{-7}/\mathrm{Mpc}^3$ in Fig. 2.8, the shape of the spectra differs considerably even at lower energies. Thus for small source densities, the best-fit parameter for α and the quality of the fit has to be determined for each combination of β and n_s separately and the relation (2.14) is not valid anymore.

From results presented in Figs. 2.7 and 2.8, we conclude that the power-law injection spectrum $1/E^{2.7}$ found earlier may be seen as a the combined effect of an injection spectrum $1/E^2$ predicted by Fermi acceleration and a power-law distribution of the maximal energies of individual sources with $\beta = 1.7$, if the source density is sufficiently large, $n_s \gtrsim 10^{-5}/\mathrm{Mpc}^3$. More generally, the exponent α_0 obtained from fits assuming identical sources is connected simply by Eq. (2.14) to the parameters α and β determining the power-laws of variable sources in this regime.

For completeness, we consider now the case of sources with variable luminosity. The total source luminosity can be defined by

$$L(z) = L_0(1+z)^m \theta(z_{\max} - z)\theta(z - z_{\min})\,, \tag{2.15}$$

where m parameterizes the luminosity evolution, and $z_{\min}$ and $z_{\max}$ are the redshifts of the closest and most distant sources. Usually m normalized in the way that $m = 0$ corresponds to the uniform distribution of sources in the expanding Universe. Sources in the range $2 < z < z_{\max}$ have a negligible contribution to the UHECR flux above 10^{18} eV. The value of $z_{\min}$ is connected to the density of sources and influences strongly the shape of bump and the strength of the GZK suppression [104, 105, 87].

The value of m influences the spectrum in the range 10^{18} eV $< E < 10^{19}$ eV [15], but less strongly than the parameter β from Eq. (2.13). Positive values of m increase the contribution of high-redshift sources and, as a result, injection spectra with $\alpha < 2.7$ can fit the observed data even in the case of the same $E_{\max}$ for all sources. For example, $\alpha = 2.6$ and $m = 3$ fits the AGASA and HiRes data as well as $\alpha = 2.7$ and $m = 0$ (χ^2/d.o.f. < 1). However, a good fit with $\alpha = 2$ requires a unrealistic strong redshift evolution of the sources, $m = 16$.

In the future, data of the Pierre Auger Observatory [4] and the Telescope Array [16] will restrict the parameter space of theoretical models similar to one presented here. If a clustered component or even individual sources can be identified in the future data, their spectra will allow one to distinguish between different possibilities for the injection spectrum. Intriguingly, the energy spectrum of the clustered component found by the AGASA experiment is much steeper than the overall spectrum [106]. Thus, one might speculate this steeper spectrum is the first evidence for the "true" injection spectrum of UHECR sources.

To summarize, the minimal model we proposed in ref. [93] can explain the observed UHECR spectrum for $E > 10^{18}$ eV with an injection spectrum as predicted by Fermi acceleration mechanism, $\alpha = 2$–2.2. However, in general the experimental data with index α_0 can be fitted for any value of α in the range $2 \leq \alpha \leq 2.7$ by choosing an appropriate index $\beta = \alpha_0 + 1 - \alpha$ in Eq. (2.13). The best-fit injection spectrum with $\alpha_0 = 2.7$ found for $E_{\max} = \text{const.}$ appears in our model as an effective value that takes

into account the averaging over the distribution of $E_{\max}$ values for various sources. This model automatically takes into account that the number of sources, which can accelerate UHECR protons to highest energies $E > 10^{20}$ eV is minimal, and most of sources accelerate UHECR protons to lower energies.

In the next section we will discuss secondary photons and neutrinos created in proton interactions with CMBR and other soft photon backgrounds.

2.5 GZK photons and neutrinos

The UHECR protons in the interaction with CMBR background produce pions. From the decay of $\pi^{\pm}$ one obtains neutrinos. These "cosmogenic neutrinos" (sometimes called these days "GZK neutrinos") have been extensively studied, from 1969 [107] onward and constitute one of the main high energy signals expected in neutrino telescopes [63]. From the decay of π^0 we obtain photons, "GZK photons", with about 10% of the original proton energy, which have been known to be a subdominant component of the UHECR since the work of Wdowczyk *et al.* in the early 1970's [108]. In 1990 it was suggested that, if the extragalactic radio background and magnetic fields are small ($B < 3 \times 10^{-11}$ G), GZK photons could dominate over protons and explain the super-GZK events [109]. The dependence of the GZK photon flux on extragalactic magnetic fields was later studied in Ref. [110]. The argument of Ref. [109] and its dependence on extragalactic magnetic fields was again discussed [69] in connection with the possible correlation of UHECR arrival directions with BL Lacertae objects [34]. Finally, an extensive study of the expected fluxes of GZK photons was done in our recent work [111] and GZK neutrinos in our works [112, 113], which I will summarize in this section.

All results in this section are based on an implicit transport code that evolve the spectra of nucleons, $\gamma-$rays, electrons, electron-, muon-, and tau-neutrinos, and their

anti-particles along straight lines. Arbitrary injection spectra and redshift distributions can be specified for the sources and all relevant strong, electromagnetic, and weak interactions have been implemented. For details see Refs. [70, 72, 114, 112].

One can ask two separate questions on GZK photon flux. First of them is: "Can GZK photons under certain conditions play a role in the formation of the UHECR spectrum?". In particular, can they explain AGASA excess? If yes, then which price we need to pay for that? Second question is: "How big is GZK photon flux under conservative assumptions about spectrum in case of existence of GZK cutoff." And can we detect it in future or not? For GZK neutrinos most interesting question is comparison of predicted neutrino fluxes with sensitivities of present and future experiments. Let us answer those questions one by one.

2.5.1 Propagation of UHECR photons and neutrinos

First, let us discuss on which parameters depends the photon flux at ultra-high energies $E > 10^{19}$ eV. For single photons with 10^{19} eV $< E < 10^{21}$ eV the main energy losses process is $e^{\pm}$ pair production on the radio background (while at lower energies pair production on the CMBR is more important). Unfortunately experimental value for radio background is unknown due to the strong foreground of our Galaxy for all small frequencies $\nu < 10$ MHz [115]. In ref. [111] we considered the three different estimates of the radio background: the minimal background of Clark et al. [115] and the two estimates of Protheroe and Biermann [116], both larger than the first one. As shown in Fig. 4 of ref. [111] the final GZK photon flux varies within factor 3 at energies below $E < 10^{20}$ eV and up to one order of magnitude at higher energies $E > 10^{20}$ eV depending on the radio background. The typical propagation length in radio background is 1-10 Mpc, depending on photon energy.

Secondary electrons and positrons also lose their energy due to synchrotron radiation in extragalactic magnetic fields. In Fig. 5 of ref. [111] it is shown that GZK

flux does not depend strongly on the magnetic field for $B_{\rm EGMF} < 10^{-10}$ G, and that for larger fields there is a suppression of the photon flux at energies $E < 10^{19}$ eV (due to pair production on the CMB followed by synchrotron energy loss).

For $E > 10^{21}$ eV the dominat energy loss process for photons is double pair production, with typical path length 100 Mpc [70]. This fact makes very important dependence of the resulting photon flux on proton maximum energy. If proton energy is large as $E > 10^{21}$ eV, photon can propagate up to 100 Mpc. As result, the photon spectrum strongly depends on the original spectrum of protons and on the distribution of sources Eq. (2.16). Most important parameters are maximum energy of proton spectrum $E_{\rm max}$, power law index of proton flux α and minimum distance to sources $z_{\rm min}$ in Eq. (2.16). Dependence of GZK photon flux on those parameters shown in Figs. 1-3 of ref. [111].

In the next section we will combine all existing constrains on protons, photon and neutrinos to show their internal connections.

2.5.2 Experimental constrains on proton, photon and neutrinos fluxes.

Let us parameterize the power law injection spectra of protons per comoving volume in the following way:

$$\phi(E, z) = f\, E^{-\alpha} \Theta(E_{\rm max} - E) \tag{2.16}$$

where f is the normalization that has to be fitted to the data. The free parameters are the spectral index α, the maximal energy $E_{\rm max}$ and three parameters of evoulution of sources in Eq. (2.15): the minimal and maximal redshifts $z_{\rm min}$, $z_{\rm max}$, and the luminosity evolution index m. Note, that parameter L_0 in Eq. (2.15) is not independent and can be combined with f.

In Fig. 2.9 we present an example in which we try to maximize both secondary neutrino and photon fluxes from GZK interactions of protons. Injection proton flux

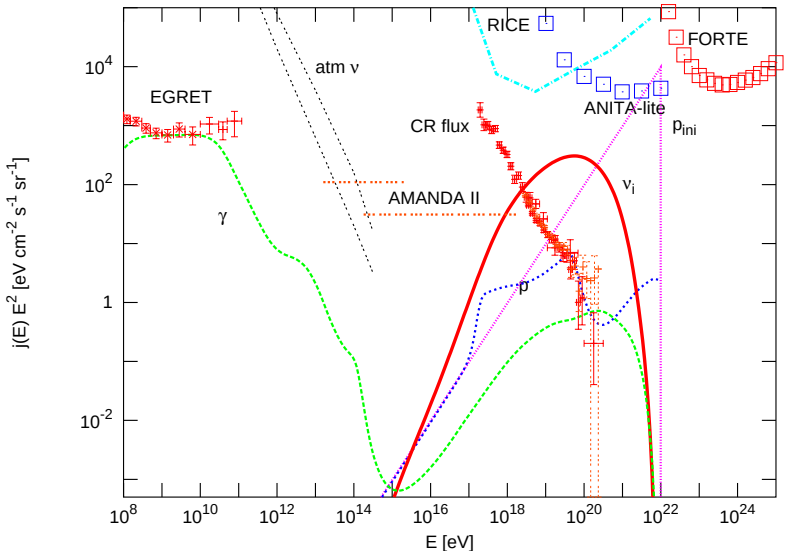

Fig. 2.9: Proton flux before propagation (majenta line) and after propagation (blue line), secondary photons (green line) and neutrinos (red line) in the scenario with maximal cosmogenic neutrino flux and high GZK photon flux per flavor as obtained by tuning the parameters of the proton primaries in Eq. (2.16) to $z_{\max} = 3$, $E_{\max} = 10^{22}$ eV, $m = 0$, $\alpha = 1$. Also shown are predicted and observed cosmic ray and $\gamma-$ray fluxes, the atmospheric neutrino flux [120], as well as existing upper limits on the diffuse neutrino fluxes, AMANDA II [121], RICE [122] and ANITA prototype experiment [66] and the limits obtained with the FORTE satellite [123], as indicated. The cosmic ray data of AGASA and HiRes are shifted together to intermediate energy scale, EGRET flux is shown to the left.

presented by the magenta line in Fig. 2.9 in this case peaked at highest energies as in AGN core acceleration models described in Section 2.1.1. We took extreme value for maximum proton energy $E_{\max} = 10^{22}$ eV in Eq. (2.16) with the purpose to illustrate constraints on neutrino and photon fluxes.

Proton flux from sources distributed as $(1+z)^3$ over redshifts $0 < z < 3$ after propagation in CMBR is shown with blue line. This flux has to be normalized on measured flux of UHECR below GZK cutoff, for which we choose AGASA and HiRes data scaled together, shifting AGASA down by 15% and HiRes up on 20 %.

When one fix the proton flux normalization with UHECR spectrum, secondary photon and neutrino fluxes can not be shifted anymore. The green line shows the photon flux. One can see that most of the photon energy cascade down to 100 MeV - 10 GeV energy range, where diffuse gamma-ray flux was measured by EGRET satellite [117, 118]. Already EGRET measurement strongly constrain parameter space of UHECR models, however in Fig. 2.9 we conservatively assume that most of gamma-ray flux in EGRET measurement is really diffuse flux. In reality a large fraction of it can be flux from large number unresolved sources, which will strongly increase constrains on diffuse photons and as result on GZK process. This issue will be checked by the next generation GLAST satellite [119] which will be launched in 2007. GLAST will be on two orders of magnitude more sensitive in compare to EGRET in energy range 10 MeV - 100 GeV.

Remaining UHECR photons at $E > 10^{19}$ eV cann't significantly contribute in the EGRET region, but they can play role in formation of UHECR spectrum, in particular contribute to AGASA excess (see next section for details).

Neutrino flux in Fig. 2.9 is shown with red line. One can see that sensitivities of present neutrino experiments does not constrain even such extreme GZK neutrino flux. However, future neutrino experiments will have a sensitivity better by one or two orders of magnitude and will able to constrain or detect GZK neutrino flux, see details in Section 2.5.6.

2.5.3 Fit of the AGASA excess at $E > 10^{20}$ eV with UHECR photons?

Now we can answer questions on the role of GZK photons, following ref. [111]. Let us investigate if GZK photons can explain AGASA flux with $E > 10^{20}$ eV or not?

In Fig. 2.10 we fit AGASA data with 3 components. First, a low energy component (LEC) which can consist from galactic iron and/or extragalactic protons with steeply falling spectrum, parameterized as $1/E^{2.7}\ \exp(-E/E_{cut})$, where $E_{cut} \sim 10^{19}$ eV and

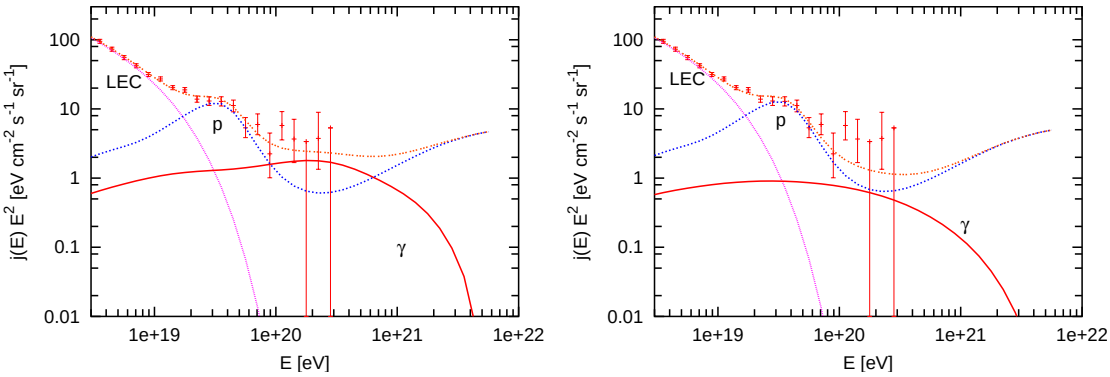

Fig. 2.10: Example of a fit of the AGASA data with extragalactic protons, the GZK photons they produce and a low energy component (LEC) at $E < 10^{19}$ eV. (a) Here we try to **maximize** the photon component thus we take an extragalactic proton spectrum $\sim 1/E$ with maximum energy $E_{\rm max} = 10^{22}$ eV, $B_{\rm EGMF} = 10^{-11}$ G and the minimum radio background. (b) same, but with reduced GZK photon flux due to assuming the intermediate extragalactic radio background.

amplitude of spectrum are parameters to fit low energy AGASA data. Second, the extragalactic protons have here an initial spectrum $\sim 1/E$, with maximum energy $E_{\rm max} = 10^{22}$ eV. Third is GZK photon flux, which is produced during the propagation of extragalactic protons.

Fit at energies below GZK cutoff $E < 10^{20}$ eV is acceptable: $\chi^2 = 14/(15-3)$, where 15 is number of energy bins and 3 is number of parameters in fit.

The fit to the super-GZK AGASA events in Fig. 2.10a is perfect, due to the GZK photons: it has a minimum $\chi^2 = 2.6$ for 3 degrees of freedom and at $E > 10^{20}$ eV there are 11.5 events (6.8 photons and 4.5 protons) where AGASA has observed 11. However, the spectrum predicts 4 events (2 photons and 2 protons) at energies above $2.5{\times}10^{20}$ eV, where AGASA has seen none which we take as barely acceptable (the probability is small, 1.8%). Larger $E_{\rm max}$ or lower α values would lead to predict even more events where AGASA has seen none and would therefore not fit well the AGASA spectrum any longer.

The fit to the super-GZK AGASA events in Fig. 2.10b, where we try to lower the

GZK flux, is not as good as that in Fig. 2.10a: it has a minimum $\chi^2 = 5.5$ for 3 degrees of freedom and at $E > 10^{20}$ eV there are 7 events (2.5 photons and 4.5 protons). But, this fit is better than that is Fig. 2.10a above the end-point of the AGASA spectrum: it predicts only 2.7 events above the highest energy AGASA point, which has a 6.7% Poisson probability.

As we see, a good fit to the AGASA data at $E > 10^{20}$ eV with GZK photons is strongly restricted by the total number of events on one side and by the number of events above the end-point of the AGASA spectrum on the other. Thus, Figs. 2.10ab provide an estimate of the maximum and minimum GZK photon flux which fit the AGASA data.

Note also that the price for explaining AGASA excess with GZK photons is assumption that protons can be accelerated up to $E_{\max} = 10^{22}$ eV ! This cann't be provided by any existing acceleration mechanism due to energy losses. Also extragalactic magnetic field and radio background should be small, but still in parameter range of existing models. Thus we conclude that under above extreme conditions one can fit AGASA data at $E > 10^{20}$ eV with GZK photons, however parameter space of model is strongly restricted and the fit is not very good.

2.5.4 GZK photon flux in a conservative model

Now, let us go to the opposite extreme and try to find the minimal GZK photon flux, following ref. [111].

In Fig. 2.11 we fit the HiRes data with a conservative model with a soft extragalactic proton spectrum, which does not require any low energy component. Thus, the power law index of the required proton spectrum is fixed by the observed UHECR at energies below 10^{19} eV, where the spectrum is $\sim 1/E^{2.7}$. This model has practically no freedom in the choice of the proton flux power law index α, although this could be slightly varied in the range $\alpha = 2.4 - 2.7$ by changing the redshift dependence of

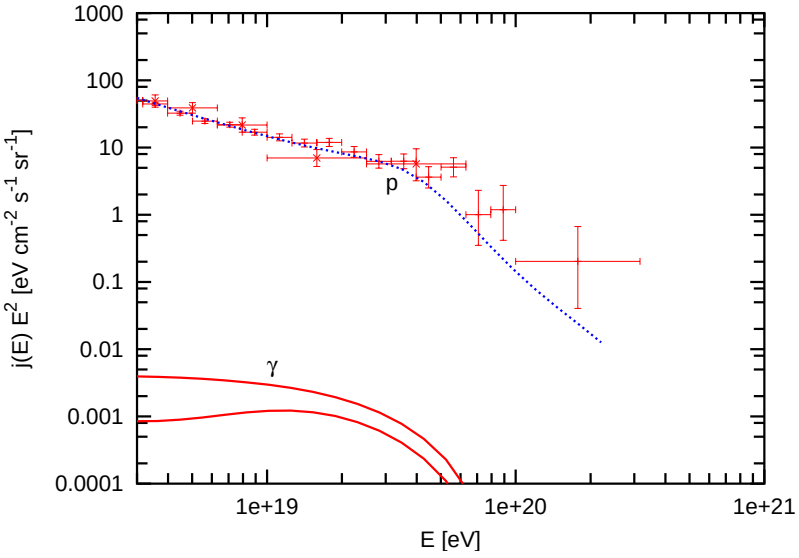

Fig. 2.11: Example of a fit to the HiRes data with extragalactic protons. Here we try to minimize the photon component thus we take an extragalactic proton spectrum $\sim 1/E^{2.7}$ with maximum energy $E_{\max} = 3\times10^{20}$ eV, maximum radio background and $B_{\rm EGMF} = 10^{-9}$ G for the lower photon curve ($B_{\rm EGMF} = 10^{-11}$ G and intermediate radio flux for the higher photon curve). The total flux is dominated by nucleons at all energies and is lower than the HiRes data at high energies. This is about the best fit that can be done to the HiRes spectrum with a proton dominated flux.

the distribution of sources. For Fig. 2.11 we conservatively choose $\alpha = 2.7$ and the smallest cutoff energy which still provides a good fit, which is $E_{\max} = 3\times10^{20}$ eV. We assume zero minimal distance to the sources (larger values do no provide a good fit to observed flux at high energies), and, to maximize the absorption of photons, the maximum radio background and $B_{\rm EGMF} = 10^{-9}$ G for the lower photon curve. We also give the result for $B_{\rm EGMF} = 10^{-11}$ G and intermediate radio background (higher photon curve) to show how the photon flux increases with a less absorbing intervening background. The total flux is insensitive to the GZK photon contribution.

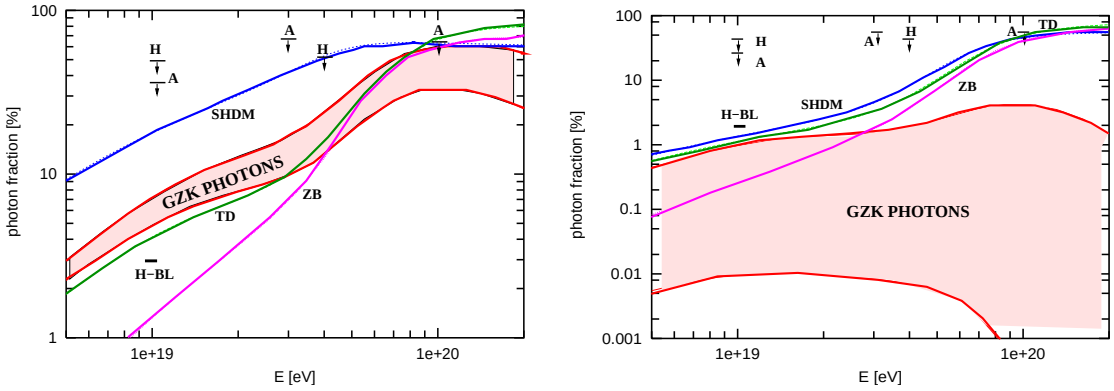

Fig. 2.12: Photon fraction in percentage of the total predicted integrated UHECR spectrum above the energy E for (a) the AGASA spectrum (left panel) and (b) the HiRes spectrum (right panel). The pink regions show the range of GZK photon fractions expected if only nucleons are produced at the sources (see Sect. III). The curves labeled ZB (Z-bursts), TD (topological defects-necklaces) and SHDM (Super Heavy Dark Matter model) show examples of minimum photon fractions predicted by these models. Upper limits: **A** from AGASA, Ref. [124] at $1-3\times10^{19}$ eV, Ref [20] and obtained with AGASA data at 10^{20} eV); **H** from Haverah Park [19]; **H-BL** show the fraction of HiRes stereo events required to explain a correlation with BL Lac sources [38, 37].

2.5.5 Photon fraction in the UHECR flux

In this section we will be more general and will take into account UHECR photon contributions from several exotic models which will be discussed in Section 3. This will allow us to compare all possible contributions to the photon flux at ultra-high energies with existing and future experimental limits on the UHECR photon flux (see more details in ref. [111]).

In Fig. 2.12a and b the AGASA spectrum and the HiRes spectrum are assumed, respectively.

The pink bands show the range of GZK photon fraction. The range of GZK photon fluxes which AGASA spectrum with $E > 10^{20}$ eV in Fig. 2.12a corresponds to the GZK photon fluxes in Fig. 2.10a and b. Case of the minimal GZK photon flux in HiRes case from Fig. 2.11 corresponds to the lower part of pink band in

Fig. 2.12b. Upper part of this band came from fitting HiRes spectrum with a steep proton spectrum $1/E$ instead of $1/E^{2.7}$.

Notice how the GZK photon band depends on the assumed spectrum: the band for AGASA is above the band for HiRes, entirely separated from it (vertical scale in the Fig. 2.10a different from one of the Fig. 2.10b). Recall that in order to obtain this band we fitted the assumed UHECR spectrum with primary protons, the GZK photons the produce, and, when needed, a galactic or extragalactic low energy component which is negligible at energies 3 $\times 10^{19}$ eV and above. If there is another component in the UHECR besides these assumed, the GZK photon fractions we obtained are only upper bounds.

The ZB, TD and SHDM curves in Fig. 2.12 correspond to the Z-burst (Section 3.5), topological defects or necklaces (Section 3.3) and super heavy dark matter (Section 3.4) models. Let us note that one does not need exotic models for fit of $E > 10^{20}$ eV part of HiRes spectrum, however, we do it here in order to treat the general case in case when the future measurements of AUGER with high statistics will settle down on some spectrum between present AGASA and HiRes measurements at $E > 10^{20}$ eV.

Notice that at energies close to 10^{20} eV, where the top-down models should dominate the flux (otherwise they are irrelevant as explanation of the UHECR), the photon fractions they predict are high, above 50% and cannot be made lower. Thus, the photon fraction at energies close to 10^{20} eV, is a crucial test for Top-Down models. This fraction is already in conflict with experimental limits discussed in Section 1.3, especially with the combined limit of AGASA and Yakutsk experiments, which restrict photon fraction to 36 % [21]. The same limit constrains a large part of the parameter space of GZK photons which try to explain AGASA excess.

To explain a correlation of BL Lac objects with the HiRes data at 10^{19} eV, a 3% fraction of neutral particles is required [38]. If these neutral particles are photons the

level required is denoted by $\mathbf{H-BL}$ at $E = 10^{19}$ eV in Fig. 2.12. If future observations confirm the HiRes-BL Lac correlation, it is very unlikely that the required neutral particles are photons, because the minimum distance to BL Lac objects is thought to be about 100 Mpc. In order to reach us, photons emitted at the source should have 10^{23} eV of energy, and, if the photons are GZK photons, the initial nucleons should be emitted at the source with even higher energies which is completely unrealistic.

To summarize, present constrains on the photon fraction at $E > 10^{20}$ eV strongly restrict if not exclude exotic models which explain the AGASA excess with UHECR photons. In case all UHECR with $E > 10^{20}$ eV are protons one can expect existence of the secondary GZK photon flux from pion production on radio background. The value of this flux strongly depends on the UHECR spectrum at highest energies and can vary by many orders of magnitude. Possible detection of this flux will help to understand properties of UHECR sources and unknown extragalactic radio background.

Note that the statistics of Auger experiment after 55 years of observation will allow to detect even 1/10000 GZK photon flux fraction at $E \sim 10^{19}$ eV which is most pessimistic case in Fig. 2.12b. However possibility to recognize such photon on large background of proton events is an open question at the moment. For more optimistic, 1 % of photon fraction Auger will easy find GZK photon flux.

2.5.6 GZK neutrinos

Few years after the famous papers on GZK cutoff [5], Berezinsky and Zatsepin realized that pions produced by primary protons will give potentially observable flux of secondary neutrinos, which they called "cosmogenic" neutrinos [107].

As one can see from Fig. 2.9 the amplitude of cosmogenic or GZK neutrino flux related to initial proton spectrum and has nothing to do with the observed UHECR spectrum and establishing possible limit(s) on GZK neutrino flux becomes non-trivial

task. Already in 1975 Berezinsky and Smirnov realized that measurement of the gamma-ray flux in the GeV region will restrict GZK neutrino flux [125] (note that the EGRET measurement of this flux was done 15 years later). Reason for restriction on the neutrino flux is in pion production. In GZK process, protons produce either π^0 and protons or π^+ and neutrons. Charged pions after decay give part of their energy to neutrinos, while neutral pion decay in two photons. As we discussed in previous section, most of the photons will cascade down in energy until they propagate through the Universe practically without interactions, which is true for photons with $E < 1$ GeV energies. Resulting total energy in GeV photons will be of the same order as the total energy in GZK neutrinos. Thus any restriction on GeV photons will put a bound on GZK neutrino flux. When the EGRET experiment found a value of the diffuse gamma-ray flux [117], Coppi and Aharonian stated that this bound restricts maximum possible GZK neutrino flux at the level of 10^3 eV/(cm^2 s sr) [126].

However later Waxman and Bahcall argued that the neutrino flux can be restricted at a value which is two orders of magnitude lower [127]. They considered $1/E^2$ proton flux and normalized it to the observed UHECR flux. In this case GZK photon flux can not exceeds value of UHECR flux around GZK cutoff, i.e. 10 eV/(cm^2 s sr). This value became very popular and got the name of "Waxman-Bahcall bound". However, two years later Mannheim, Protheroe and Rachen found contra-example, which violate the Waxman-Bahcall bound. They took a proton flux as $1/E$ and showed that they could get much larger values of the neutrino flux [128]. However they derived their own limit which still was more restrictive then original value dictated by EGRET limit.

In our paper ref. [112] we numerically investigated parameter space for this model varying all parameters in Eq. (2.16). We found that the Waxman-Bahcall bound and even the Mannheim, Protheroe and Rachen bound are just model-dependent calculations and one can easy violate both of them, varying parameters of the pro-

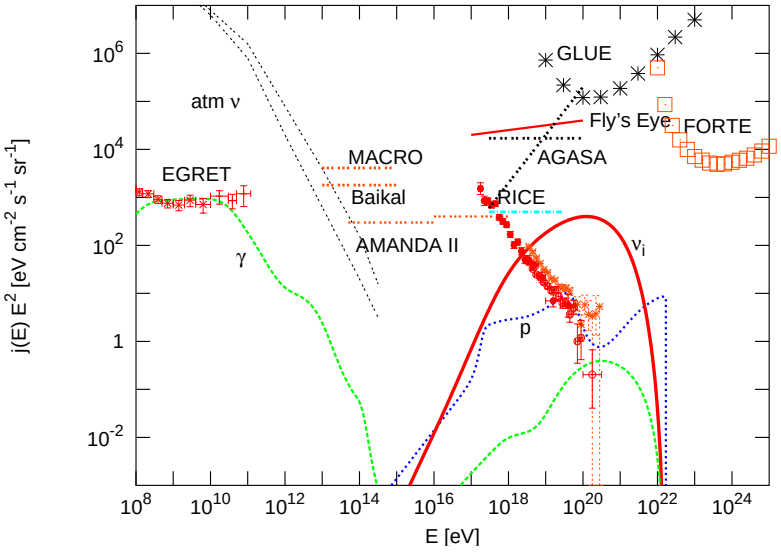

Fig. 2.13: Proton flux after propagation (blue line), secondary photons (green line) and neutrinos (red line) in the scenario with maximal cosmogenic neutrino fluxes per flavor as obtained by tuning the parameters of the proton primaries in Eqs. (2.16-2.15) to $z_{\max} = 2$, $E_{\max} = 2 \times 10^{22}\,\mathrm{eV}$, $m = 0$, $\alpha = 1$. Also shown are predicted and observed cosmic ray and $\gamma-$ray fluxes, the atmospheric neutrino flux [120], as well as existing upper limits on the diffuse neutrino fluxes from MACRO [129], AMANDA II [54], BAIKAL [60], AGASA [130], the Fly's Eye [131] and RICE [122] experiments, and the limits obtained with the Goldstone radio telescope (GLUE) [133] and the FORTE satellite [123], as indicated. The cosmic ray data of AGASA and HiRes, EGRET flux is shown to the left.

ton injection spectra and the distribution of sources. Our final conclusion was that only real limit on GZK neutrino flux is old limit on GeV photon flux from EGRET experiment.

In this section we will follow ref. [112] and compare the GZK neutrino flux with limits from present and future neutrino experiments. We will assume for simplicity that all three neutrino flavors are maximally mixed thus have equal fluxes. This is an excellent approximation for our purpose. For each flavor we sum fluxes of particles and anti-particles. The resulting neutrino spectra depend insignificantly on $z_{\min}$ in

Eq. (2.16) in the range $0 \leq z_{\rm min} \lesssim 0.1$ where local effects could play a role, and thus we will set $z_{\rm min} = 0$ in the following. To obtain the maximal neutrino fluxes for a given set of values for all these parameters , we determine the maximal normalization f in Eq. (2.16) by demanding that both the accompanying nucleon and $\gamma-$ray fluxes are below the observed cosmic ray spectrum and the diffuse $\gamma-$ray background observed by EGRET, respectively.

The two major categories of high energy neutrino experiments are based on detection in water, ice or underground, typically sensitive below $\simeq 10^{16}\,$eV, and on air shower detection, usually sensitive at higher energies. Existing neutrino flux upper limits come from the underground MACRO experiment [129] at Gran Sasso, AMANDA II [54] in the South Pole ice, and the Lake BAIKAL neutrino telescope [60] in the first category, and the AGASA ground array [130], the former fluorescence experiment Fly's Eye [131], the Radio Ice Čerenkov Experiment RICE [122] (there is also a limit from the HiRes experiment [132] which is between the RICE and AGASA limits), the Goldstone Lunar Ultra-high energy neutrino experiment GLUE [133], and the Fast On-orbit Recording of Transient Events (FORTE) satellite [123] in the second category. As an example, an optimistic cosmogenic neutrino flux is compared with current neutrino flux upper limits in Fig. 2.13. One can see that sensitivities of the present experiments cann't restrict the GZK neutrino flux.

The cosmogenic neutrino flux models are compared with future sensitivities in Fig. 2.14. Future experiments in the first category include NT200+ at Lake Baikal [60], ANTARES [61], NESTOR in Greece [62], as well as a possible common km^3 scale detector in the Mediterranean [135, 134], and ICECUBE [64], the next-generation version of AMANDA at the South pole. The air shower based category includes the Pierre Auger project [55], the telescope array [56], the fluorescence/Čerenkov detector NUTEL [57], and the space based EUSO [136].

Most promising are sensitivities of ANITA [65] and Auger [55], which are 100 times

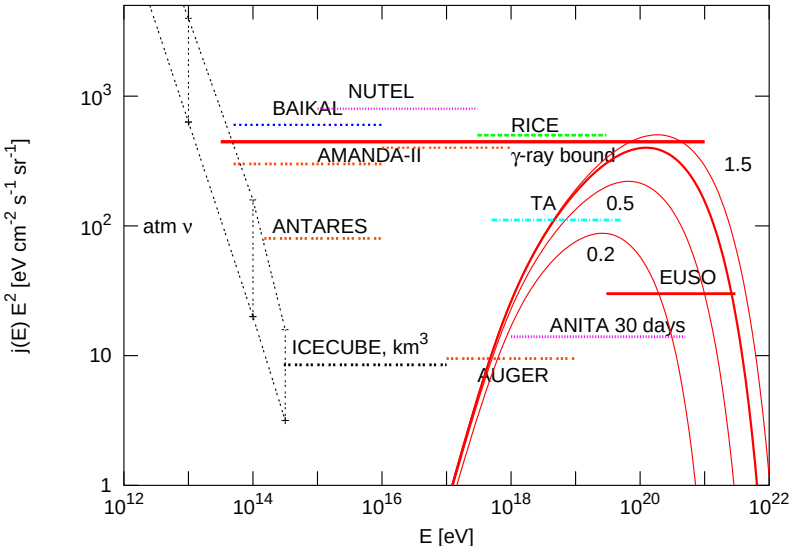

Fig. 2.14: The cosmogenic neutrino flux per flavor shown in Fig. 2.13 (thick line) and flux reduced in 2 or 5 times in comparison with expected sensitivities of the currently being constructed Pierre Auger project to tau-neutrinos [55], the planned projects telescope array (TA) [56], the fluorescence/Čerenkov detector NUTEL [57], the space based EUSO [136], the water-based Baikal [60] and ANTARES [61] (the NESTOR sensitivity for 1 tower would be similar to AMANDA-II and for 7 towers similar to ANTARES [62]), the ice-based AMANDA-II [54] and ICECUBE [64] (similar to the intended Mediterranean km^3 project [134]), and the radio detectors RICE [122] and ANITA [65], as indicated. All sensitivities except for ANITA and RICE refer to one year running time. For comparison, the $\gamma-$ray bound derived from the EGRET GeV $\gamma-$ray flux [118] is also shown.

below gamma-ray bound. In principle, they will be able to detect GZK neutrinos with realistic proton maximum energy $E_{\max} \sim 3 \times 10^{20}$ eV. Even if they will establish just limits, those limits strongly restrict parameters of injection proton spectrum and as result will restrict acceleration mechanism.

The original Auger limit [55] was calculation using only the ground detector. In our recent paper ref. [137] we made a similar calculation for Auger fluorescence detectors. Unfortunately, the sensitivity of the Auger fluorescence detectors in several

times worthier in compare to ground array and one can detect UHE neutrinos in this way only in very optimistic scenarios.

Finally let us note that it is possible to put a low limit on the GZK neutrino flux in the same way as we tried with GZK photon flux. This was done in ref. [138] by fitting the UHECR flux with protons and calculating possible flux range for GZK neutrinos in Fig. 5 of ref. [138]. The lowest expected value for GZK neutrino flux is at the level of 1eV/(cm^2 s sr) [138]. Again, athors assumed that all the observed UHECR are protons. If all highest energy UHECR are iron nuclei both GZK neutrino and photon fluxes would go to zero.

3. EXOTIC UHECR MODELS

In the Introduction we discussed several hints in the UHECR data which require physics beyond Standard Model for their explanation. The two most important of them are:

- The excess of events with $E > 10^{20}$ eV above the GZK cutoff in AGASA experiment [1]. More general: Existence of UHECR with $E > 10^{20}$ eV with no sources within 50 Mpc within few degrees from arrival directions [8].
- The possible correlations of the HiRes stereo data with BL Lac objects [38, 37].

All other significant features in UHECR data can be explained within Standard Model of elementary particles. Historically, excess in the AGASA data was found 12 years ago [139], which caused large interest to the models which can explain it with different kind of physics beyond Standard Model. Those models can be divided in 3 major groups. In the first group, it is assumed that UHECR with $E > 10^{20}$ eV are secondaries from decays of new heavy particles, which either were created by topological defects or constitute Dark Matter. The second group of models assumes that there is a new particle, which can propagate on larger distance compared to protons. Finally, one can keep only the Standard Model particles, but change the physical laws. For example, assuming that Lorentz invariance is violated, one can prevent protons to interact with CMBR [140]. Or one can assume that neutrinos become strongly interacting particles at very high energies [141]. The remaining model, which stays separately, is the Z-burst model. Formally it does not assume the

existence of any new physics to explain AGASA data, however as we will show below it violates several astrophysical constrains.

Correlations of HiRes stereo data with BL Lac objects was sfound very recently [38, 37] (see also Introduction). The main problem is that the correlated objects are located too far in order that neutrons or even photons can reach us. But neutral particles, which can propagate from distant BL Lacs exist in most of models which tried to explain AGASA excess above GZK cutoff. Thus most of those models except for Super Heavy Dark Matter and top-down models can also explain correlation of HiRes data with BL lac objects.

Below I will discuss five exotic models, including models with new hadrons, model with axion-like particles, top-down model, model of Super-Heavy Dark Matter and Z-burst model.

3.1 New hadrons

The general idea of this model is that new hadrons with mass larger than the proton mass $M > 1$ GeV would have GZK cutoff at higher energies, depending on mass value, because threshold energy is proportional to hadron mass, Eq. (2.6).It was first suggested by G. Farrar [142, 143]. Supersymmetric (SUSY) models with a strongly interacting particle as lightest supersymmetric particle (LSP) or next-to-lightest SUSY particle (NLSP) are very interesting for explaining the AGASA excess above the GZK cutoff. Hadrons containing a gluino as UHECR primaries were first suggested by Farrar [142, 143]. This model with a light gluino together with a light photino as cold dark matter candidate is meanwhile excluded [144, 145]. However, more general models with a light gluino or a light sbottom quark are still viable. Despite existing of such particles, one needs to obey several constrains on their properties in order to explain the AGASA data above cutoff or correlations with BL Lacs. In our

paper [104] a model-independent, purely phenomenological approach was developed, which we will follow in this section.

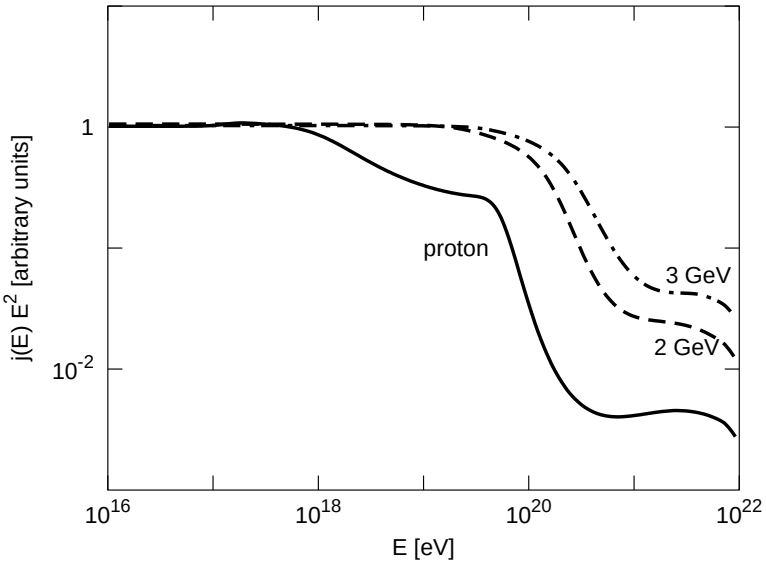

Fig. 3.1: Energy spectrum of new hadrons X^0 calculated with an injection spectrum E^{-2} and uniformly distributed sources for a $M_X = 2$ and 3 GeV; for a comparison the proton spectrum is also shown. At energies 10^{18} eV $< E < 6 \times 10^{19}$ eV the proton spectrum is also suppressed due to e^+e^- production.

First of all let us discuss how GZK cutoff changes with hadron mass M_X. For electrically neutral hadrons X^0 with masses $M_X = 2$ and 3 GeV, an injection spectrum E^{-2} and uniformly distributed sources, the spectrum after propagation in intergalactic space is shown in Fig. 3.1. For comparison we show also the similar spectrum for protons. One can see that e^+e^- pair production changes the proton spectrum shape as compared to neutral hadrons. Besides, the cutoff value is shifted to higher energies, proportionally to thehadron mass, Eq. (2.6). Moreover, due to smaller cross section and smaller energy losses in single pion production (m_π/M_X smaller for $M_X > M_P$) the GZK cutoff is much less pronounced in the case of new hadrons.

However, one can not have a mass of the new hadron randomly high. Since the

observed extensive air showers (EAS) are consistent with simulated EAS initiated by protons, any new primary proposed to solve the GZK puzzle has to produce EAS similar to those of protons. The simplest way to do it is to require that the new primary is strongly interacting and haa s relatively small mass $M_X < 3$ GeV [146].

Another important condition is that the particle X should be stable, traveling through the Universe. The lifetime t_X should be bigger then

$$t_X = \frac{R_U}{c}\frac{M_S}{E_{\rm UHE}} \approx 12 \text{ days } \frac{R_U(\text{Gpc})M_X(\text{GeV})}{E_{20}} , \tag{3.1}$$

where R is measured in Gpc, M_X in GeV and $E_{20} = E/(10^{20}\text{eV})$.

The production of new hadrons in astrophysical objects was also investigated in Ref. [104]. It was found that proton-proton collisions in astrophysical accelerators cannot produce sufficiently high fluxes of new primaries without contradicting existing measurements of photon [117] and neutrino fluxes [54, 122, 123]. In contrast, for a light shadron with mass $\lesssim 3\,\text{GeV}$ and the astrophysically more realistic case of UHE proton collisions on optical/infrared background photons in the sources there is no contradiction with existing limits. Also, the required initial proton energy is not too extreme, $E \lesssim 10^{21}\,\text{eV}$, which may be achieved by astrophysical acceleration mechanisms. The only essential condition for the sources is that they should be optically thick for protons in order to produce these new hadrons. This condition applies to all models with new particles produced by protons.

One of the important features of scenarios with new hadrons, and of any model in which the production cross section $\sigma_{p\gamma\to X}$ of a new particle x is much smaller than the total proton-photon cross section $\sigma_{p\gamma}$, is the high flux predicted for secondary high-energy neutrinos. This neutrino flux is approximately $F_{\rm CR}\sigma_{p\gamma}/\sigma_{p\gamma\to X}$ in terms of the maximal contribution of S particles to the observed cosmic ray flux, $F_{\rm CR} \simeq (E/10^{20}\,\text{eV})^{-2}$ eV/(cm^2 s sr).

Fig. 3.2 shows the neutrino flux produced in sources togeather with new hadrons.

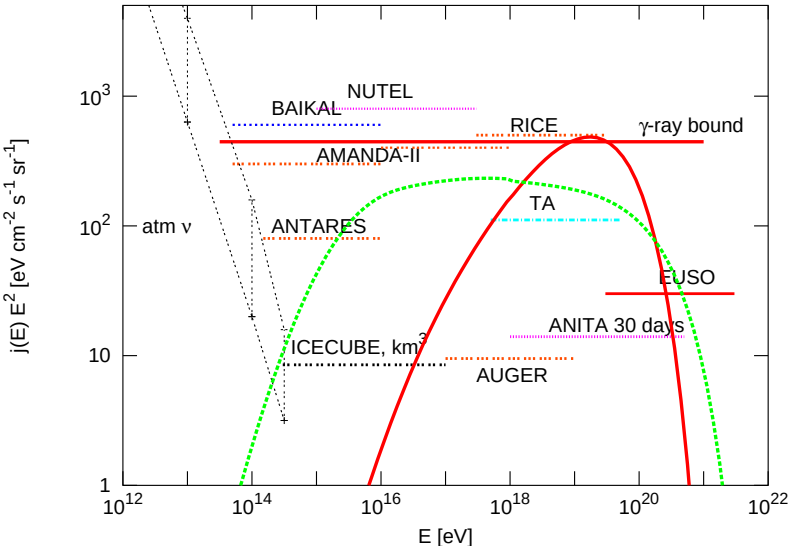

Fig. 3.2: Neutrino fluxes per flavor predicted by scenarios where UHECRs are explained as new hadrons produced as secondaries of accelerated protons with source density evolution $m = 3$ and maximum redshift of sources $z_{\max} = 2$, compared to expected experimental sensitivities. The solid line is for a flux of primary protons peaked at $E = 10^{21}$ eV and the dashed line is for a primary proton flux $\propto E^{-2}$ up to $E_{\max} = 10^{22}$ eV.

Neutrino flux for a primary proton flux $\propto E^{-2}$, restricted already with 5 years of AMANDA-II data, which is on the level of "ANTARES" line in Fig. 3.2. From other side ANITA experiment will be able from 2007 test a peaked spectrum in Fig. 3.2 [65]. A non-observation of neutrinos in the near future will make impossible to render the production cross section of the new hadrons consistent with existing limits in these scenarios.

3.2 Axions

The original idea of our work ref. [147] was to consider standard Peccei-Quinn axions as messenger particles which can be converted in distant source sites from UHECR

photons, and can be converted back to UHECR photons nearby or in our Galaxy. Unfortunately even the coherent conversion and back-conversion between photons and axions in large-scale magnetic fields is not enough to produce the required flux. However, one may construct models of other novel (pseudo)scalar neutral particles with properties that would allow for sufficient rates of particle production in the source and shower production in the atmosphere to explain the observations. As an explicit example for such particles in ref. [147] we considered light sgoldstinos in SUSY models.

Many bounds on axion-like particles arise from cosmology, astrophysics and laboratory measurements [148, 149]. Still, there remain regions in parameter space where X particles can explain UHECRs without contradicting these limits.

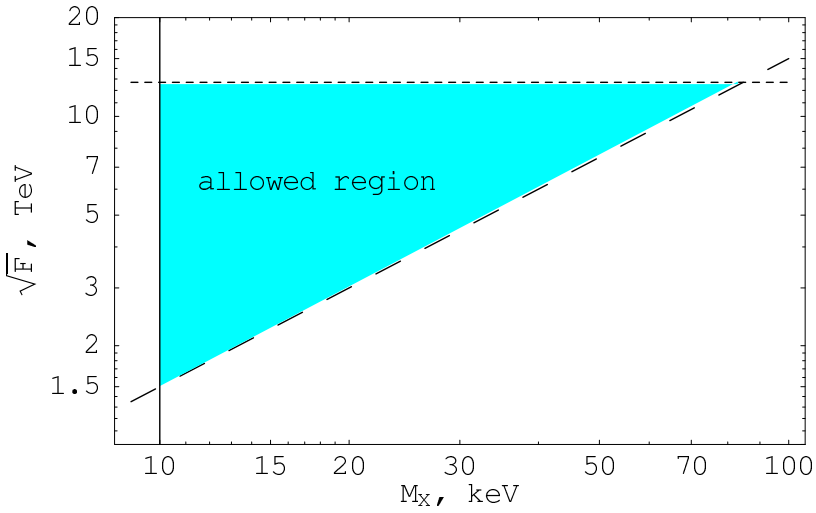

Fig. 3.3: Allowed region for the sgoldstino mass and the suppersymmetry breaking scale $(M_X, \sqrt{F})$. The short-dashed line corresponds to the limit (3.3), the long-dashed line to (3.2). Sgoldstinos with masses less than 10 keV (vertical solid line) are ruled out by the helium-burning life-time of horizontal-branch stars [151].

In ref. [147] we presented a specific SUSY example of axion-like particle – light sgoldstinos. A variety of experimental limits on models with light sgoldstinos has

been derived in [150]. Additionally, in order to explain UHECR data with $E > 10^{20}$ eV they have to obey several conditions. They would propagate through universe without decay if

$$\sqrt{F} \gtrsim 1.5 \text{ TeV} \left(\frac{10^{20} \text{ eV}}{E_X}\right)^{1/4} \frac{M_X}{10 \text{ keV}} \tag{3.2}$$

where M_X is sgoldstino mass, E_X its energy and $\sqrt{F}$ is the supersymmetry breaking scale. Same condition guarantees the absence of a GZK cutoff for the sgoldstinos [147].

The condition that sgoldstinos can be produced in the source and interact in atmosphere in similar way as protons is:

$$\sqrt{F} \lesssim 13 \text{ TeV} \left(\frac{E_X}{10^{20} \text{ eV}}\right)^{1/4} \tag{3.3}$$

In Fig. 3.3 we presented allowed parameter space of sgoldstinos. The short-dashed line corresponds to the limit (3.3), the long-dashed line to (3.2). Sgoldstinos with masses less than 10 keV (vertical solid line in Fig. 3.3) are ruled out by the helium-burning life-time of horizontal-branch stars [151].

We note that our allowed region in Fig. 3.3 suggests that the supersymmetry breaking scale is $\sqrt{F} \sim$ 1–10 TeV. Hence our light sgoldstino model can be tested in searches for rare decays of J/ψ and Υ and in reactor experiments (for details see Ref. [150]). This low scale of supersymmetry breaking may be also tested at new generation accelerators like LHC.

Let us finally note that same model can explain correlations of HiRes data with BL lac objects, contrary to the model discussed in the next section.

3.3 Top-down model

Historically, top-down (TD) scenarios were proposed as an alternative to acceleration scenarios to explain the huge energies up to 3×10^{20} eV observed in the cosmic ray spectrum. In these top-down scenarios UHECRs are the decay products of some

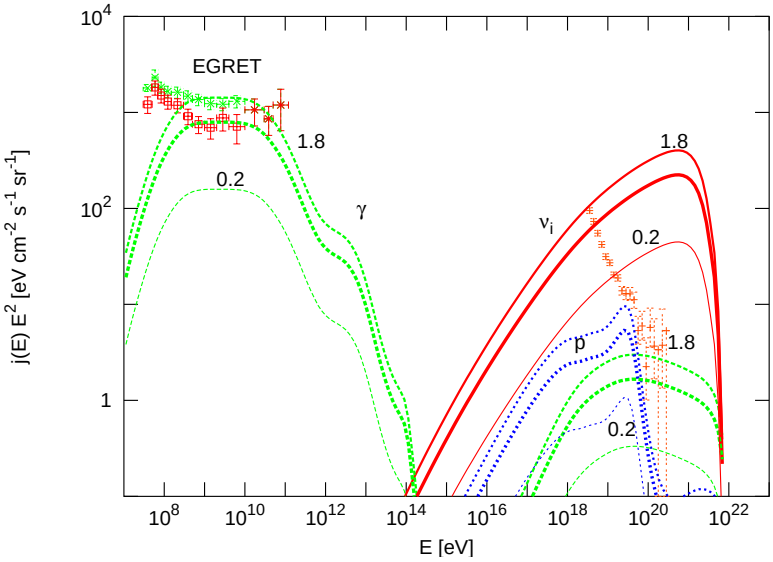

Fig. 3.4: Flux predictions for protons, photons and neutrinos for a TD model with $m_X = 2 \times 10^{13}\,\mathrm{GeV}$. The contribution of photons and protons to the UHECR flux decreases with decreasing fractional contribution to the diffuse photon flux at EGRET energies which is denoted in numbers. Even a TD contribution to the present estimate of the diffuse EGRET flux [117, 118] as high as 100% (unlabeled thick curves) is only marginally consistent with the AGASA UHECR excess. .

super-massive "X" particles of mass $m_X \gg 10^{20}\,\mathrm{eV}$ close to the grand unified scale $10^{15} - 10^{16}$ GeV, and have energies all the way up to $\sim m_X$. Thus, the massive X particles could be meta-stable relics of the early Universe with lifetimes of the order the current age of the Universe 15 Gyr or could be released from topological defects that were produced in the early Universe during symmetry-breaking phase transitions predicted by in Grand Unified Theories (GUTs). The X particles typically decay into leptons and quarks. The quarks hadronize, producing jets of hadrons which, together with the decay products of the unstable leptons, result in a large cascade of energetic photons, neutrinos and light leptons with a small fraction of protons and neutrons, some of which contribute to the observed UHECR flux. The resulting injection spectra have been calculated from QCD in various approximations, see Ref. [9] for a review

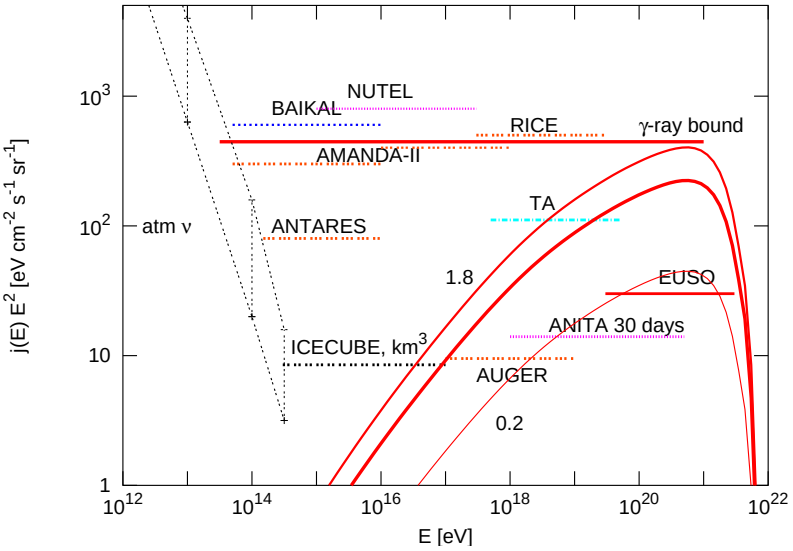

Fig. 3.5: Neutrino fluxes per flavor predicted by the three normalizations of the TD model of Fig. 3.4 compared to future experimental sensitivities.

and Ref. [152] for more recent work. In Fig. 3.4 we used the QCD spectra discussed in Ref. [153] and shown in Fig. 11 of Ref. [114]. Calculations for modern decay spectra discussed in ref. [152] are even less consistent with the AGASA data due to the relatively smaller fraction of photons at highest energies.

Fig. 3.4 shows the secondary proton, photon and neutrino fluxes for $m_X = 2 \times 10^{13}\,\mathrm{GeV}$, $B = 10^{-12}\,\mathrm{G}$, and the moderately low theoretical estimate from Ref. [116]. These parameters lead to optimistic neutrino fluxes for the maximal normalization consistent with all data. Fig. 3.4 shows that already the improved upper limit on the true diffuse photon background by EGRET implies a UHECR flux too small compared to the AGASA excess at energies $E \gtrsim 10^{20}\,\mathrm{eV}$. The parameters used in the figure represent the "best fit point" for this model; in particular for all other masses m_X the disagreement is more severe. The new EGRET upper limit [118] thus strongly disfavor extragalactic top-down scenarios. New experiment GLAST [119] can

significantly improve EGRET limit, making this argument even stronger. In addition, independently of this problem of overproduction of GeV $\gamma-$rays, a non-observation of TD neutrinos by future neutrino experiments will rule out the possibility that extragalactic top-down mechanisms significantly contribute to the UHECR flux, as can be seen when comparing Fig. 3.5 and Fig. 3.4.

3.4 Super-Heavy Dark Matter

A possible explanation of the AGASA excess for $E > 10^{20}$ eV would be the existence of superheavy dark matter (SHDM) [154, 155]. Superheavy particles with mass $M_X \sim 10^{13-14}$ GeV can be naturally produced during inflation and would be today the dominant component of dark matter [156]. Such particles will concentrate in galactic halos and the secondaries from their decay could be responsible for the highest energy cosmic rays. Note however that if SHDM is significant part of Dark Matter, reproduction of UHECR flux require fine tuning of decay rate. It has also been suggested that not decays but annihilation of SHDM particles produce the observed UHECRs [157].

By construction, this model has a clean signature: the dominance of photons at the highest energies [154]. Fraction of photons and protons in SHDM decay or annihilation spectrum is almost equal in modern detailed analysis it [152], while old calculations used ratio 1 proton for 10 photons [154]. Recent limit from AGASA and Yakutsk data restrict photon fraction at highest energies $E > 10^{20}$ eV as low as 36 % [21]. Thus even in case of 50 % photon fraction at highest energies $E > 10^{20}$ eV SHDM is in conflict with photon limit.

Another signature of the SHDM scenario is the spatial anisotropy of the expected signal predicted due to the non-central position of the Sun in our Galaxy [158]. Since UHECR experiments in the northern hemisphere do not see the Galactic center, they are not very sensitive to a possible anisotropy of arrival directions of UHECR from

SHDM. In contrast, the Galactic center was visible for the old Australian SUGAR experiment [159]. The anisotropy of the arrival directions using data from the full sky was discussed in Refs. [160, 161]. Reference [160] compared the flux from the Galactic center to the one from the anti-center and found them to be comparable. Similarly, the full-sky harmonic analysis including AGASA and SUGAR data from Ref. [161] found no significant anisotropy.

In the work [162] we used a two-component energy spectrum of UHECRs consisting of protons from uniformly distributed astrophysical sources and the fragmentation products of SHDM calculated in SUSY-QCD, see Fig. 3.6a. We compare their expected arrival direction distribution to the data of the SUGAR experiment using a Kolmogorov-Smirnov test. Contrary to the harmonic analysis, this test allows to quantify directly the (dis-) agreement of the measured distribution of arrival direction with the expected one in the SHDM model. We considered both decays and annihilations of SHDM. Note that similar analysis for SHDM component only was independently done in ref. [163].

In Fig. 3.6b, we show the dependence of the probability that SUGAR data are consistent with SHDM model on the energy cutoff for decaying SHDM. The important parameter, which characterize expected anisotropy is the core radius in Dark Matter profile of our Galaxy, for which we take here the realistic value $R_c = 15$ kpc. Dependence of the probability on the core radius is shown in Fig. 5 of ref. [162]. The two thick solid lines in Fig. 3.6b show probability P for a combination of SHDM and uniform sources. The upper one corresponds to an injection spectrum $1/E^{2.3}$, the lower one to an injection spectrum $1/E^{2.7}$, presented in Fig. 3.6a. The probability P for the assumption that all UHECR are extragalactic protons shown with thin solid line. Its behavior suggest that the minimum for $E_{\rm min} \sim 7 \times 10^{19}$ eV is a fluctuation coming from small number of events similar to the maximum around $E_{\rm min} \sim 5 \times 10^{19}$ eV. In the range $E_{\rm min} \sim (3-4) \times 10^{19}$ eV, the fluctuations adding an

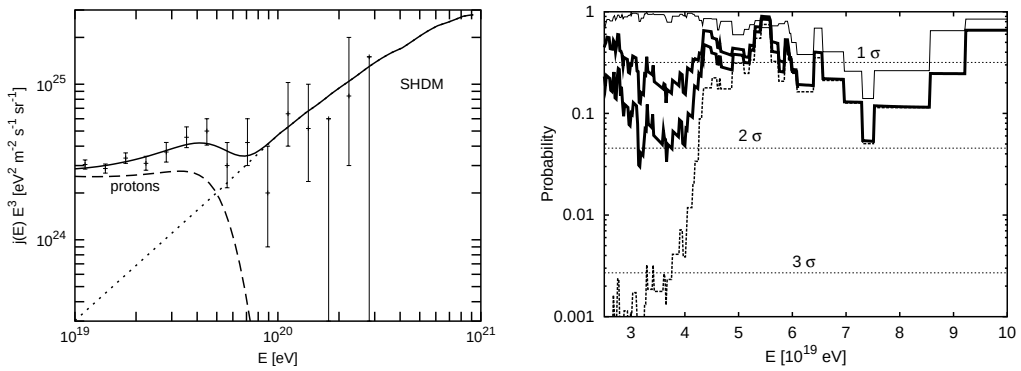

Fig. 3.6: a. Fit of UHECR spectrum by extragalactic protons with injection spectrum $1/E^{2.7}$ and SHDM. b. Dependence of the probability on the energy cutoff in the SUGAR data for decaying SHDM. Two thick solid lines corresponds to extragalactic protons with the injection spectrum $1/E^{2.3}$ (lower line) and $1/E^{2.7}$ (upper line). Dashed line correspond to assumption that all SUGAR UHECR above give energy are due to SHDM. Thin solid line correspond to assumption that all SUGAR data due to extragalactic protons.

additional event are relatively small. Therefore, we considered the probability in this range as more reliable indicator for the consistency of SHDM with the SUGAR arrival directions; we conclude that the SUGAR data have the probability $p = 5 - 20\%$ to be consistent with the SHDM depending on the injection spectrum of the extragalactic protons. Note, that one cann't assume that the SHDM gives significant contribution to the observed UHECR flux at energies $E < 4 \times 10^{19}$ eV. Dashed line in Fig. 3.6b show that this scenario excluded at 3 σ level.

Contrary to decaying SHDM, the annihilation scenario is disfavored at least at 99% CL by the SUGAR data, while SHDM contribution at $E < 4 \times 10^{19}$ eV excluded in this case at 5 σ level [162].

We conclude that the SHDM scenario is therefore disfavored by present experimental data, both by limits on photon fraction and by isotropy in arrival directions of observed cosmic rays. It will be finally tested by the Pierre Auger experiment in the

near future. In principle, already first dataset of Auger data with statistic, similar to AGASA will allow to test this model much better then old SUGAR data.

3.5 Z-burst model

The only known Standard Model particle that is able to travel from high redshift sources, $z \geq 1$, is the neutrino. The mean free path of very energetic neutrinos with respect to the resonance production of Z-boson by scattering on the cosmic neutrino background (CNB) larger then the horizon size [164]. Indeed, to excite the Z-resonance the energy of the ultra high energy (UHE) neutrinos should be equal to:

$$E_{UHE} = m_Z^2/2E_{CNB} \approx 4 \cdot 10^{21} \text{ eV}(1 \text{ eV}/E_{CNB}) \tag{3.4}$$

where E_{CNB} is the energy of the cosmic background neutrinos. If they are massless then $\langle E_{CNB} \rangle \approx 3T_\nu \approx 5 \cdot 10^{-4}$ eV. For massive neutrinos with $m_\nu > T_\nu$, $E_{CNB} = m_\nu$, from neutrino oscillations we know that at least for two of them last case applied.

The energy averaged cross-section is

$$\bar{\sigma}_Z = \int (ds/M_Z^2)\sigma(\bar{\nu}\nu \to Z) = 2\pi\sqrt{2}G_F = 4 \cdot 10^{-32}\,\text{cm}^2 \tag{3.5}$$

Because of the resonant nature of the process the cross-section contains only first power of G_F and is much larger than typical weak interaction cross-sections. The mean free path of UHE neutrinos with respect to this reaction is

$$l_{free} = 1/(\sigma_Z n_\nu) \approx 5 \cdot 10^{29} \text{ cm}\,(n_\nu/55\text{cm}^{-3})^{-1} \approx 75 \text{ Gpc } (n_\nu/110\text{cm}^{-3})^{-1} \tag{3.6}$$

where n_ν is the neutrino number density; it is normalized to the standard average cosmological number density of neutrinos $n_\nu^{(0)} = 110/\text{cm}^3$. Thus, most of UHE neutrinos travel through all Universe without interactions.

In this model a possible source of UHECR events could be the decay of Z-boson produced by very energetic neutrinos annihilated on CNB within 100 Mpc from our

Galaxy. The primary energetic neutrinos could be produced by astrophysical sources at very large distances. This explanation was suggested in the papers [165].

The first self-consistent calculation of the Z-burst model was done in ref. [166]. It was assumed there that the distribution of neutrino sources evolves with redshift as $(1+z)^3$ or in the way similar to the evolution of active galaxies. It was shown that in this case the secondary photons with energies $E < 100$ GeV would overshoot the measured EGRET flux several times. This means that the "Z-burst" mechanism in its simplest version contradicts the data.

A possible solution to this problem is to increase the local neutrino densities by a factor $N > 20$ on scales $l \sim 5$ Mpc [166]. The probability of neutrino interactions would locally increase and for the same flux of UHECR (normalized to the experimental data) the secondary electromagnetic flux in the EGRET region of energies would be below the measured values. However, our Local Group of galaxies has a too small mass $M = 4 \times 10^{12}\ M_{\rm sun}$ to provide a significant clustering of neutrinos with $m_\nu < 2$ eV on factor more them few [167].

In our paper Ref. [114] its was suggested simple solution for this problem, which is a redistribution of neutrino sources with redshift. Already in case of uniformly distributed sources $(1+z)^0$ the EGRET bound of photon flux can be satisfied [114].

However, this does not save the Z-burst model in case of realistic astrophysical sources. Indeed, neutrinos are usually produced together with photons in pion decays. As already discussed in this thesis, the total power in neutrinos in such production mechanism is of the order of total power in photons. Photons usually cascade down in energy in sources up to GeV-TeV energy range, where they should again satisfy the EGRET limit. In Fig. 3.7 from ref. [114] we show exactly this case. One can see that EGRET flux is overshoted by two orders of magnitude. The conclusion of ref. [114] was that sources for Z-burst model should emit preferably neutrinos. As was shown later in more detailed source analysis, no astrophysical accelerator exists that meets

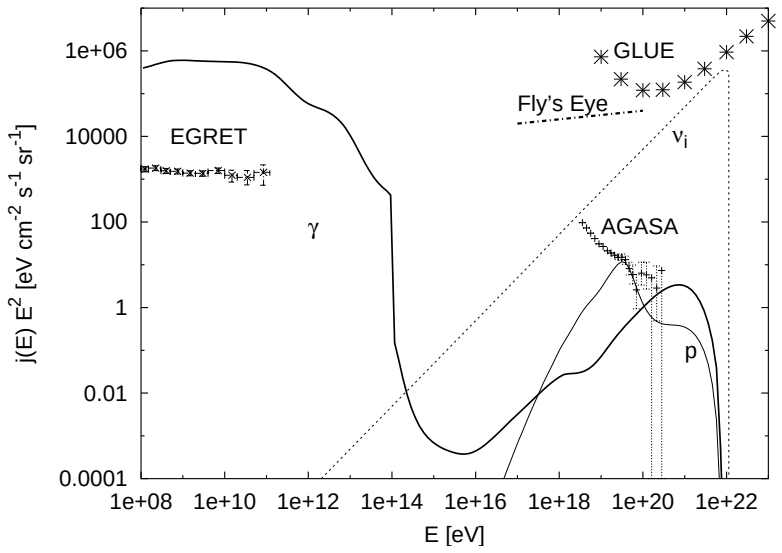

Fig. 3.7: Fluxes of photons (think solid line), neutrinos (dotted line) and secondary protons (thin solin line) for sources emitting equal power in neutrinos and $\gamma-$rays with $E < 100$ TeV (from ref. [114]).

the requirements of the Z-burst model [168].

In principle, neutrino flux in Z-burst model strongly depends on neutrino mass through resonance condition Eq. (3.4). In ref. [169] it was suggested that neutrino mass can be defined from Z-burst model even with some precision $m_\nu = 0.26 + 0.20 - 0.14$ eV, if this model itself is working. As was shown in our ref. [114] this statement was not correct. Authors of ref. [169] fixed many unknown parameters on their favorite values and made their fit to UHECR spectrum varying only neutrino mass. In ref. [114] we show in Fig. 2ab that by varying unknown parameters one can easy fit UHECR spectrum for any neutrino mass in range 0.1 eV $< E <$ 1 eV with equally good fit.

Thus Z-burst model can only theoretically work for exotic pure neutrino emitting sources. However already in 2003 new limits on neutrino flux from the radio exper-

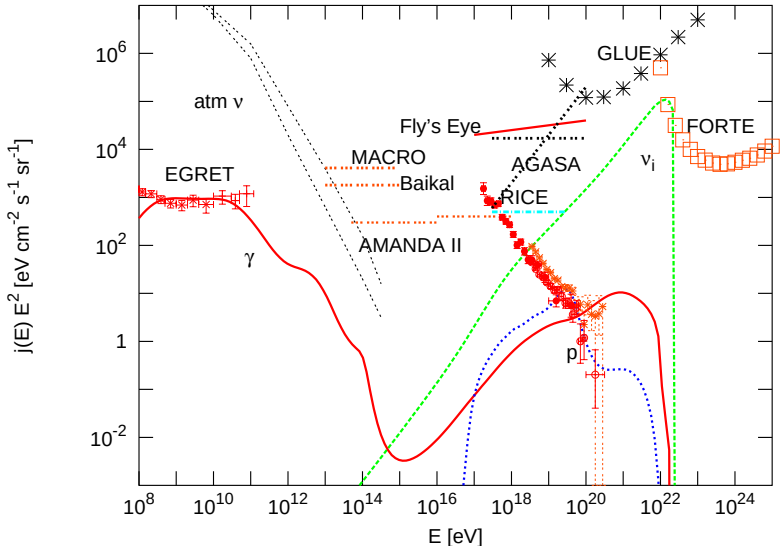

Fig. 3.8: Flux predictions for a Z-burst model averaged over flavors and characterized by the injection parameters $z_{\rm min} = 0$, $z_{\rm max} = 3$, $\alpha = 1$, $m = 0$, $E_{\rm max} = 3 \times 10^{22}\,$eV in Eq. (2.16) for neutrino primaries instead of protons. The sources are assumed to be exclusive neutrino emitters. All neutrino masses were assumed equal with $m_\nu = 0.33$ eV and we again assumed maximal mixing between all flavors.

iment FORTE [123] exclude part of the parameter space for Z-burst model. Right after arrival of FORTE data we found in ref. [113] that the parameter space excluded by FORTE data corresponds to low neutrino masses $m_\nu < 0.3$ eV. At the same time a combination of cosmological data including the WMAP experiment limit the sum of the masses of active neutrinos to $\lesssim 1\,$eV [170]. Solar and atmospheric neutrino oscillations indicate that individual neutrino masses are nearly degenerate on this scale [171], and thus the neutrino mass per flavor must satisfy $m_\nu \lesssim 0.33\,$eV.

For the maximal possible value of the neutrino mass $m_\nu \simeq 0.33\,$eV the neutrino flux required for the Z-burst model was only in marginal conflict with the FORTE upper limit [123], as shown in Fig. 3.8. For all other cases the conflict is considerably more severe. Also note that this argument does not depend on the shape

of the low energy tail of the primary neutrino spectrum which could thus be even monoenergetic, as could occur in exclusive tree level decays of superheavy particles into neutrinos [172]. However, in addition this possibility has been ruled out by overproduction of GeV $\gamma-$rays due to loop effects in these particle decays [173].

Finally, let us note that more recent experimental data from GLUE [174] and ANITA prototype [66] experiments established even more strong limits on neutrino flux in compare to FORTE, and completely closed the window in the parameter space of Z-burst model. Now we can conclude that Z-burst model is ruled out from neutrino data and this is the first example when UHECR neutrino experiments are able to restrict exotic UHECR models, existing otherwise. We hope that future data of ANITA, Auger, ICECUBE and km^3 experiments will allow us not only exclude exotic models but also detect finally extragalactic neutrino flux at highest energies.

4. SUMMARY

In this section I would like to summarize the main ideas and results presented in this thesis. The work starts with an Introduction on Ultra-High Energy Cosmic Ray (UHECR) experimental data. It is followed by two Chapters, one devoted to explanations of UHECR data within Standard Model of particle physics and other to the exotic models, which try to explain experimental hints beyond Standard Model.

In Chapter 1.1 I gave summary of the present experimental situation in UHECR physics. Now it is a very interesting time when old generation of experiments, like ground based AGASA and fluorescence HiRes are finished or almost finished their work while new generation of hybrid detectors like Pierre Auger Observatory or Telescope Array will present their results in near future. In discussion of experimental results I tried to pay attention to the most interesting hints in data which, if confirmed in future, will require new physics for their explanation.

In Section 1.2 I presented spectra of UHECR measured by AGASA and HiRes experiments and shown two important features. First, both spectra are completely consistent at all energy scales up to 10^{20} eV after have performed a 30-35 % of global energy shift (HiRes up or AGASA down). Second, after this shift, the disagreement between the two experiments at the highest energies becomes statistically insignificant at the level of 2 σ. Conservatively, the AGASA excess at highest energies can be explained by a statistical fluctuation or by a systematic effect, which can be, for example, the increase of the energy of UHECR showers due to atmospheric electric fields during thunderstorms.

In Section 1.3 recent results on UHECR chemical composition was presented. It was shown that at high energies $E > 5 \times 10^{18}$ eV the spectrum is dominated by protons, while at lower energies $E < 10^{18}$ eV primaries mostly are iron nuclei. There was no indication found for UHECR photons. The most important is recent limit from AGASA and Yakutsk experimental data, which restrict fraction of photons at the level 36% at highest energies $E > 10^{20}$ eV.

In Section 1.4 I presented two important anisotropy signals in present data on arrival directions of cosmic rays. The first of them is the clustering of UHECR at small scales 2.5 degrees. The AGASA experiment sees such a signal with a probability of 10^{-3} while HiRes see no signal. Here for the first time I combined AGASA data with HiRes after a proper shift in energy by 35 %. Combined dataset gave similar significance of the signal to AGASA data along. This issue has to be investigated with future bigger datasets. The second signal is the clustering of UHECR at moderate scales 10-30 degrees when combining all existing experiments, which has a formal probability 10^{-4}, which reduces to 3×10^{-3} after taking penalty for scan over angle. This signal, if confirmed will be the first signature of connection between cosmic rays and Large Scale Structure.

Finally, in Section 1.5 I briefly discussed searches of UHECR sources. The most intriguing result at the moment is the possible correlation of HiRes data with BL lac objects, which can happen with probability order of 10^{-4}. If this signal is confirmed by future data, it will require a new physics to explain such correlations.

Chapter 2 is devoted to Standard Model description of UHECR data. In this chapter it is assumed that all hints beyond Standard Model in experimental data are just fluctuations.

In Section 2.1 I discuss the acceleration of protons to highest energies and accompanying gamma-ray and neutrino signals. A particular model for acceleration of UHECR protons by electric field in vicinity of Black Hole in cores of Active Galactic

Nuclei (AGN) is discussed in Section 2.1.1. The next section describes how large scale 100 kpc jets, observed in AGNs can be formed by secondary UHE photons, produced by protons in AGN cores. Accompanied neutrino flux is discussed in the following sections. First, I discuss the neutrino flux from GeV EGRET sources, then I show that observations of neutrinos from popular TeV sources will restrict neutrino production mechanism to $p + A$ collisions rather than to $p + \gamma$ interactions.

Section 2.2 is devoted to the propagation of UHECR protons in the intergalactic medium. There are two important ingredients of propagation, first, the energy loss mechanisms, including the famous GZK cutoff, $e^{\pm}$ pair production and redshifting and second, deflections in the extragalactic and galactic magnetic fields.

Connection between small scale clustering signal and density of UHECR sources is discussed in Section 2.3. It is shown that AGASA data are consistent with the density of sources n similar to one of bright AGNs $n_{\rm AGN} \sim 2 - 4 \times 10^{-5}/{\rm Mpc}^3$.

In Section 2.4 it was described how one can explain the observed spectrum $1/E^{2.7}$ by hard proton spectra $1/E^2$ predicted by shock acceleration mechanisms, if one relax the usual assumption of identical sources and take into account distribution of their maximum energy. This idea finalized the construction of a minimal model, which explains all UHECR with $E > 10^{18}$ eV by protons from extragalactic sources.

Section 2.5 is one of the central in this thesis. I discussed secondary photon and neutrinos from UHECR proton propagation. In future combined efforts of UHECR experiments, neutrino telescopes and gamma-ray experiments will help us to understand nature of cosmic rays at highest energies and find their sources.

I start from details of propagation of UHE gamma-rays and neutrinos. Then I show how one can fit AGASA excess beyond GZK cutoff with secondary photons from GZK interactions. Unfortunately, such a mechanism requires unrealistic assumptions on proton acceleration up to 10^{22} eV or even higher energies. Next, contrary to previous case, I derive minimal GZK photon flux, under the assumption that all

UHECR at highest energies are protons. In this case photons consist only of 10^{-4} of UHECR at energies $E > 10^{19}$ eV.

In next Section I compare the UHE photon fraction predictions in several models with existing experimental limits. It is shown that 36 % limit on photon fraction at energies $E > 10^{20}$ eV from AGASA and Yakutsk experiments strongly disfavor exotic model which predict large photon flux at highest energies, including Super Heavy Dark Matter, top-down models and Z-burst model.

In final part of this chaper I discuss predictions for the GZK neutrino flux and compare them to sensitivities of the present and future neutrino experiments. It is shown that next generation experiments like ICECUBE, ANITA and Auger will be able to see GZK neutrino flux in optimistic scenarios.

Chapter 3 is devoted to five exotic models, which all originally tried to explain AGASA excess at highest energies. Three of them, model of new hadrons, model of axion-like particles and Z-burst model can also explain possible correlations of HiRes arrival directions with BL lac sources. I discussed the present status of all those models.

In Section 3.1 model of new hadrons considered phenomenologically. This mean that even at the moment there is no any good candidate for such particle, one can suppose that it exist and try to make self-consistent model with it. In this Section I discuss production of those particles in astrophysical objects, their propagation to Earth and interactions in atmosphere.

Model for axion-like particles was discussed in Section 3.2. For supersymmetric version of such particles sgoldstinos it is derived parameter space which consistent with all restrictions existence, production, propagation and interactions of such exotic particles.

Section 3.3 devoted to so-called top-down models. It is shown that constrains from diffuse gamma-ray background measured by EGRET strongly restrict this model,

making explanation of AGASA excess for it very problematic.

The Super Heavy Dark Matter model, which together with AGASA excess pretended to explain Dark Matter signal is discussed in the Section 3.4. It is shown that even the old SUGAR experiment disfavor annihilation version of this model. Besides it is restricted by the limit on photon fraction from AGASA and Yakutsk experiments.

In final Section 3.5 I discussed the Z-burst model, which is the only exotic model which pretends to explain AGASA excess above GZK cutoff within Standard Model physics. Instead this model required existence of exotic "pure neutrino sources" to not contradict the EGRET bound on diffuse photon flux. However, even in this case this model is excluded by limits on diffuse neutrino flux from FORTE, GLUE and Anita-lite experiments in combination with limit on neutrino masses from cosmology.

ACKNOWLEDGMENTS

I would like to thank my collaborators, including Felix Aharonian, Carla Aramo, Graciela Gelmini, Dmitry Gorbunov, Antonio Insolia, Michael Kachelriess, Oleg Kalashev, Alex Kusenko, Vadim Kuzmin, Andrew Leonardi, Genaro Miele, Andrey Neronov, Lorenzo Perrone, Ofelia Pisanti, Georg Raffelt, Gunter Sigl, Igor Tkachev and Maria Tortola for fruitful common work on Ultra High Energy Cosmic Rays, Gamma-rays and Neutrinos. Additionally I would like to thank Vadim Kuzmin, who encouraged me to start working in this interesting field. Also I would like to give special thanks to my wife Ksenia for her kind support.

BIBLIOGRAPHY

[1] M. Takeda *et al.*, Astropart. Phys. **19**, 447 (2003) [astro-ph/0209422].

[2] R. U. Abbasi *et al.*, Phys. Rev. Lett. **92**, 151101 (2004) [astro-ph/0208243]; D. R. Bergman [the HiRes Collaboration], astro-ph/0507484.

[3] M. Nagano *et al.*, J. Phys. **G10**, 1295 (1984).

[4] J. Abraham *et al.* [Pierre Auger Collaboration], Nucl. Instrum. Meth. A **523**, 50 (2004). http://www.auger.org/

[5] K. Greisen, Phys. Rev. Lett. **16**, 748 (1966); G. T. Zatsepin and V. A. Kuzmin, JETP Lett. **4**, 78 (1966) [Pisma Zh. Eksp. Teor. Fiz. **4**, 114 (1966)].

[6] A. Kusenko and D. Semikoz, Phys. Rev. D **70**, 121303 (2004) [arXiv:hep-ph/0410313].

[7] P. Sommers *et al.* [Pierre Auger Collaboration], astro-ph/0507150.

[8] J. W. Elbert and P. Sommers, Astrophys. J. **441**, 151 (1995) [arXiv:astro-ph/9410069].

[9] P. Bhattacharjee and G. Sigl, Phys. Rept. **327**, 109 (2000) [astro-ph/9811011]; see also G. Sigl, Science **291**, 73 (2001) [astro-ph/0104291] for a short review.

[10] S. P. Knurenko *et al.*, astro-ph/0411484.

[11] D. J. Bird *et al.* [HIRES Collaboration], Astrophys. J. **424**, 491 (1994).

[12] D. J. Bird *et al.* [HIRES Collaboration], Astrophys. J. **424** (1994) 491.

[13] C. T. Hill and D. N. Schramm, Phys. Rev. D **31**, 564 (1985).

[14] V. S. Berezinsky and S. I. Grigor'eva, Astron. Astrophys. **199**, 1 (1988).

[15] V. Berezinsky, A. Z. Gazizov and S. I. Grigorieva, hep-ph/0204357; astro-ph/0210095; Nucl. Phys. Proc. Suppl. **136**, 147 (2004) [astro-ph/0410650]; Phys. Lett. B **612** (2005) 147 [astro-ph/0502550].

[16] M. Fukushima, Prog. Theor. Phys. Suppl. **151** (2003) 206.

[17] T. Pierog, R. Engel and D. Heck, arXiv:astro-ph/0602190.

[18] K. Shinozaki *et al.*, Proc. 28th ICRC (Tsukuba), **1**, 437 (2003).

[19] M. Ave, J. A. Hinton, R. A. Vazquez, A. A. Watson and E. Zas, Phys. Rev. Lett. **85**, 2244 (2000) [arXiv:astro-ph/0007386]; Phys. Rev. D **65**, 063007 (2002) [arXiv:astro-ph/0110613].

[20] M. Risse *et al.*, Phys. Rev. Lett. **95**, 171102 (2005) [arXiv:astro-ph/0502418].

[21] G. I. Rubtsov *et al.*, arXiv:astro-ph/0601449.

[22] M. Risse [Pierre Auger Collaboration], arXiv:astro-ph/0507402.

[23] M. Takeda *et al.*, "Small-scale anisotropy of cosmic rays above 10**19-eV observed with the Akeno Giant Air Shower Array," Astophys. J. **522** 225 [astro-ph/9902239];

[24] M. Takeda *et al.*, Proc. 27th ICRC, Hamburg, 2001.

[25] P. G. Tinyakov and I. I. Tkachev, 'Correlation function of ultra-high energy cosmic rays favors point sources," JETP Lett. **74**, 1 (2001) [Pisma Zh. Eksp. Teor. Fiz. **74**, 3 (2001)] [astro-ph/0102101];

[26] P. Tinyakov and I. Tkachev, arXiv:astro-ph/0301336.

[27] C. B. Finley and S. Westerhoff, "On the evidence for clustering in the arrival directions of AGASA's ultrahigh energy cosmic rays," Astropart. Phys. **21**, 359 (2004) [astro-ph/0309159].

[28] R. U. Abbasi *et al.* [The High Resolution Fly's Eye Collaboration (HIRES)], Astrophys. J. **610**, L73 (2004) [arXiv:astro-ph/0404137].

[29] H. Yoshiguchi, S. Nagataki and K. Sato, "Statistical significance of small scale anisotropy in arrival directions of ultra-high energy cosmic rays," astro-ph/0404411.

[30] R. U. Abbasi *et al.* [The High Resolution Fly's Eye Collaboration], Astrophys. J. **623**, 164 (2005) [arXiv:astro-ph/0412617].

[31] One can count value of autocorrelation function in the following way: $w_A = 7$ is AGASA value, one more event in triplet region give 3, one combined AGASA-HiRes doublet exist for public dataset with $E > 4 \times 10^{19}$ eV plus one HiRes doublet seen in Fig. in ref. [30]

[32] M. Kachelriess and D. V. Semikoz, arXiv:astro-ph/0512498.

[33] A. Cuoco *et al.*, astro-ph/0510765.

[34] P. G. Tinyakov and I. I. Tkachev, JETP Lett. **74**, 445 (2001) [Pisma Zh. Eksp. Teor. Fiz. **74**, 499 (2001)] [arXiv:astro-ph/0102476].

[35] P. G. Tinyakov and I. I. Tkachev, Astropart. Phys. **18**, 165 (2002) [arXiv:astro-ph/0111305].

[36] D. S. Gorbunov, P. G. Tinyakov, I. I. Tkachev and S. V. Troitsky, Astrophys. J. **577**, L93 (2002) [arXiv:astro-ph/0204360].

[37] R. U. Abbasi *et al.* [HiRes Collaboration], arXiv:astro-ph/0507120.

[38] D. S. Gorbunov, P. G. Tinyakov, I. I. Tkachev and S. V. Troitsky, JETP Lett. **80**, 145 (2004) [Pisma Zh. Eksp. Teor. Fiz. **80**, 167 (2004)] [arXiv:astro-ph/0406654].

[39] D. S. Gorbunov, P. G. Tinyakov, I. I. Tkachev and S. V. Troitsky, arXiv:astro-ph/0508329.

[40] D. S. Gorbunov and S. V. Troitsky, Astropart. Phys. **23**, 175 (2005) [arXiv:astro-ph/0410741].

[41] D. R. Bergman *et al.*, Proc. 29th ICRC (Pune), 2005 [astro-ph/0507483].

[42] A. M. Hillas, Ann. Rev. Astron. Astrophys. **22**, 425 (1984).

[43] R. J. Protheroe and R. W. Clay, Publ. Astron. Soc. of Australia **21**, 1 (2004) [astro-ph/0311466].

[44] R. J. Protheroe, Astropart. Phys. **21**, 415 (2004) [astro-ph/0401523].

[45] A. Neronov and D. Semikoz, New Astronomy Reviews **47**, 693 (2003);

[46] A. Neronov, P. Tinyakov and I. Tkachev, J. Exp. Theor. Phys. **100**, 656 (2005) [Zh. Eksp. Teor. Fiz. **100**, 744 (2005)] [arXiv:astro-ph/0402132].

[47] A. Neronov, D. Semikoz, F. Aharonian and O. Kalashev, Phys. Rev. Lett. **89**, 051101 (2002) [arXiv:astro-ph/0201410].

[48] A. Y. Neronov and D. V. Semikoz, Phys. Rev. D **66**, 123003 (2002) [arXiv:hep-ph/0208248].

[49] K. S. Thorne, R. Price, A. Macdonald, *Black holes: the Membrane Paradigm*, Yale Univ. Press (1986).

[50] R. M. Wald, Phys. Rev. **D 10**, 1680 (1974).

[51] L. D. Landau, E. M. Lifshitz, *The Classical Theory of Fields*, Pergamon Press, (1959).

[52] F.A Aharonian, P.S. Coppi, H.J. Völk, ApJ, **423**, L5 (1994)

[53] R. C. Lamb and D. J. Macomb, Astrophys. J. **488**, 872 (1997)

[54] P. Niessen [the AMANDA Collaboration], arXiv:astro-ph/0306209; For the energy range $2.5 \times 10^{15}\,\mathrm{eV} \lesssim E \lesssim 5.6 \times 10^{18}\,\mathrm{eV}$ we rescaled the AMANDA-B10 limit from http://www-rccn.icrr.u-tokyo.ac.jp/icrc2003/PROCEEDINGS/PDF/326.pdf to AMANDA-II exposure.

[55] J. J. Blanco-Pillado, R. A. Vazquez and E. Zas, Phys. Rev. Lett. **78**, 3614 (1997) [astro-ph/9612010]; K. S. Capelle, J. W. Cronin, G. Parente and E. Zas, Astropart. Phys. **8**, 321 (1998) [astro-ph/9801313]; A. Letessier-Selvon, Nucl. Phys. Proc. Suppl. **91**, 473 (2000) [astro-ph/0009416]; X. Bertou, P. Billoir, O. Deligny, C. Lachaud and A. Letessier-Selvon, Astropart. Phys. **17**, 183 (2002) [astro-ph/0104452].

[56] M. Sasaki and M. Jobashi, astro-ph/0204167.

[57] G. W. Hou and M. A. Huang, arXiv:astro-ph/0204145.

[58] J. F. Ormes et al., Proc. 25th *International Cosmic Ray Conference*, eds.: M. S. Potgieter et al. (Durban, 1997). Vol. 5, 273; Y. Takahashi et al., Proc. of International Symposium on *Extremely High Energy Cosmic Rays: Astrophysics and Future Observatories*, ed. M. Nagano (Institute for Cosmic Ray Research, Tokyo, 1996)., p. 310; For neutrino

searches see http://www.fcp01.vanderbilt.edu/schedules/upload/ John_Krizmanic-OWL-vandy.pdf; see also D. B. Cline and F. W. Stecker, OWL/AirWatch science white paper, astro-ph/0003459.

[59] For general information see http://www.euso-mission.org.

[60] V. Balkanov *et al.* [BAIKAL Collaboration], astro-ph/0112446.

[61] For general information see http://antares.in2p3.fr; see also S. Basa, in Proc. *19th Texas Symposium on Relativistic Astrophysics*, Paris (France), eds. E. Aubourg, et al., Nuc. Phys. B (Proc. Supp.) 80B (2000). (e-print astro-ph/9904213); ANTARES Collaboration, e-print astro-ph/9907432.

[62] For general information see http://www.nestor.org.gr . See also L. Resvanis, Proc. Int.Workshop on Neutrino Telescopes, Venice 1999, vol. II, 93.

[63] C. Spiering, J. Phys. G **29**, 843 (2003) [arXiv:astro-ph/0303068].

[64] For general information see http://icecube.wisc.edu/; see also F. Halzen: Am. Astron. Soc. Meeting 192, # 62 28 (1998); AMANDA collaboration: astro-ph/9906205, Proc. *8th International Workshop on Neutrino Telescopes*, Venice, Feb. 1999.

[65] P. Gorham et al. (ANITA collaboration), http://www.ps.uci.edu/ barwick/anitaprop.pdf.

[66] S. W. Barwick *et al.* [ANITA Collaboration], arXiv:astro-ph/0512265.

[67] F. Halzen and D. Hooper, arxive:astro-ph/0502449 .

[68] R. U. Abbasi *et al.* [HiRes Collaboration], arXiv:astro-ph/0507120.

[69] O. E. Kalashev, V. A. Kuzmin, D. V. Semikoz and I. I. Tkachev, arXiv:astro-ph/0107130.

[70] S. Lee, Phys. Rev. D **58**, 043004 (1998) [astro-ph/9604098];

[71] M. J. Chodorowski,A. A. Zdziarski, M. Sikora, Astrophysical Journal **400** 181 (1992).

[72] O. E. Kalashev, V. A. Kuzmin and D. V. Semikoz, astro-ph/9911035; Mod. Phys. Lett. A **16**, 2505 (2001) [astro-ph/0006349].

[73] G. Sigl, F. Miniati and T. A. Ensslin, Phys. Rev. D **68**, 043002 (2003) [arXiv:astro-ph/0302388]; Phys. Rev. D **70**, 043007 (2004) [arXiv:astro-ph/0401084].

[74] K. Dolag, D. Grasso, V. Springel and I. Tkachev, JETP Lett. **79**, 583 (2004) [Pisma Zh. Eksp. Teor. Fiz. **79**, 719 (2004)] [arXiv:astro-ph/0310902]; JCAP **0501**, 009 (2005) [arXiv:astro-ph/0410419].

[75] M. Bruggen, M. Ruszkowski, A. Simionescu, M. Hoeft and C. D. Vecchia, Astrophys. J. **631**, L21 (2005) [arXiv:astro-ph/0508231].

[76] P. G. Tinyakov and I. I. Tkachev, Astropart. Phys. **24**, 32 (2005) [arXiv:astro-ph/0411669].

[77] M. Kachelrieß, P. D. Serpico and M. Teshima, astro-ph/0510444.

[78] D. Harari, S. Mollerach and E. Roulet, JHEP **9908**, 022 (1999) [arXiv:astro-ph/9906309].

[79] P. G. Tinyakov and I. I. Tkachev, Astropart. Phys. **18**, 165 (2002) [arXiv:astro-ph/0111305].

[80] M. Prouza and R. Smida, Astron. Astrophys. **410**, 1 (2003) [arXiv:astro-ph/0307165].

[81] E. Waxman, K. B. Fisher and T. Piran, "The signature of a correlation between $> 10^{19}$ eV cosmic ray sources and large scale structure," Astrophys. J. **483**, 1 (1997) [astro-ph/9604005].

[82] S. L. Dubovsky, P. G. Tinyakov and I. I. Tkachev, "Statistics of clustering of ultra-high energy cosmic rays and the number of their sources," Phys. Rev. Lett. **85**, 1154 (2000) [astro-ph/0001317].

[83] Z. Fodor and S. D. Katz, "Ultra high energy cosmic rays from compact sources," Phys. Rev. D **63**, 023002 (2001) [hep-ph/0007158].

[84] H. Yoshiguchi, S. Nagataki, S. Tsubaki and K. Sato, "Small scale clustering in isotropic arrival distribution of ultra-high energy cosmic rays and implications for their source candidate," Astrophys. J. **586**, 1211 (2003) [Erratum-ibid. **601**, 592 (2004)] [astro-ph/0210132].

[85] H. Yoshiguchi, S. Nagataki and K. Sato, "Arrival distribution of ultra-high energy cosmic rays: Prospects for the future," Astrophys. J. **592**, 311 (2003) [astro-ph/0302508].

[86] P. Blasi and D. De Marco, "The small scale anisotropies, the spectrum and the sources of ultra high energy cosmic rays," Astropart. Phys. **20**, 559 (2004) [astro-ph/0307067].

[87] M. Kachelriess and D. Semikoz, Astropart. Phys. **23**, 486 (2005) [arXiv:astro-ph/0405258].

[88] P. Sommers, Astropart. Phys. **14**, 271 (2001) [arXiv:astro-ph/0004016].

[89] N. Hayashida *et al.*, "Updated AGASA event list above 4*10**19-eV," astro-ph/0008102.

[90] M. Teshima, private communication.

[91] A. T. Steffen *et al.*, "The Changing AGN Population," Astrophys. J. **596**, L23 (2003) [astro-ph/0308238].

[92] R. U. Abbasi *et al.* [The High Resolution Fly's Eye Collaboration (HIRES)], Astrophys. J. **610**, L73 (2004) [astro-ph/0404137].

[93] M. Kachelriess and D. V. Semikoz, arXiv:astro-ph/0510188.

[94] C. T. Hill, D. N. Schramm and T. P. Walker, Phys. Rev. D **34**, 1622 (1986).

[95] J. P. Rachen, T. Stanev and P. L. Biermann, Astron. Astrophys. **273**, 377 (1993) [astro-ph/9302005].

[96] J. N. Bahcall and E. Waxman, Phys. Lett. B **556**, 1 (2003) [hep-ph/0206217].

[97] T. Wibig and A. W. Wolfendale, J. Phys. G **31**, 255 (2005) [astro-ph/0410624].

[98] D. Allard, E. Parizot, E. Khan, S. Goriely and A. V. Olinto, astro-ph/0505566.

[99] D. De Marco and T. Stanev, astro-ph/0506318.

[100] D. De Marco, P. Blasi and A. V. Olinto, Astropart. Phys. **20**, 53 (2003) [astro-ph/0301497].

[101] M. Lemoine, Phys. Rev. D **71**, 083007 (2005) [astro-ph/0411173].

[102] F. W. Stecker and S. T. Scully, Astropart. Phys. **23**, 203 (2005) [astro-ph/0412495].

[103] V. S. Berezinskii *et al*, Astrophysics of cosmic rays, Amsterdam: North-Holland 1990. T. Gaisser, Cosmic Rays and Particle Physics, Cambridge University Press 1991.

[104] M. Kachelriess, D. V. Semikoz and M. A. Tortola, Phys. Rev. D **68**, 043005 (2003) [arXiv:hep-ph/0302161].

[105] P. Blasi and D. De Marco, Astropart. Phys. **20** (2004) 559 [astro-ph/0307067].

[106] M. Takeda *et al.*, Proc. 27th ICRC (Hamburg), **1**, 341 (2001).

[107] V. S. Berezinsky and G. T. Zatsepin, Phys. Lett. B **28**, 423 (1969). V. S. Berezinsky and G. T. Zatsepin, Sov. J. Nucl. Phys. 11 (1970) 111 [Yad. Fiz. 11 (1970) 200].

[108] J. Wdowczyk , W. Tkaczyk, C. Adcock and A. W. Wolfendale, J. Phys. A: Gen. Phys **4** L37-9 (1971); J. Wdowczyk , W. Tkaczyk and A. W. Wolfendale, J. Phys. A: Gen. Phys **5** 1419 (1972); J. Wdowczyk and A. W. Wolfendale, Astrophys. Jour. **349**, 35 (1990)

[109] F.A. Aharonian, V.V. Vardanian and B.L. Kanevsky, Astrophysics and Space Science **167**, 111 (1990); Corresponding proton GZK cutoff calculation was done in *ibid* **93**, 111 (1990).

[110] S. j. Lee, A. Olinto and G. Sigl, Astrophys. J. **455**, L21 (1995) [arXiv:astro-ph/9508088].

[111] G. Gelmini, O. Kalashev and D. V. Semikoz, arXiv:astro-ph/0506128.

[112] O. E. Kalashev, V. A. Kuzmin, D. V. Semikoz and G. Sigl, Phys. Rev. D **66**, 063004 (2002) [arXiv:hep-ph/0205050].

[113] D. V. Semikoz and G. Sigl, JCAP **0404**, 003 (2004) [arXiv:hep-ph/0309328].

[114] O. E. Kalashev, V. A. Kuzmin, D. V. Semikoz and G. Sigl, Phys. Rev. D **65**, 103003 (2002) [arXiv:hep-ph/0112351].

[115] T. A. Clark, L. W. Brown, and J. K. Alexander, Nature **228**, 847 (1970).

[116] R. J. Protheroe and P. L. Biermann, Astropart. Phys. **6**, 45 (1996) [Erratum-ibid. **7**, 181 (1997)]

[117] P. Sreekumar *et al.*, Astrophys. J. **494**, 523 (1998) [astro-ph/9709257].

[118] A. W. Strong, I. V. Moskalenko and O. Reimer, arXiv:astro-ph/0306345.

[119] For general information see http://www-glast.stanford.edu

[120] see, e.g., P. Lipari, Astropart. Phys. **1**, 195 (1993).

[121] K. Munich [IceCube Collaboration], *Prepared for 29th International Cosmic Ray Conference (ICRC 2005), Pune, India, 3-11 Aug 2005*

[122] I. Kravchenko *et al.*, arXiv:astro-ph/0206371. I. Kravchenko, arXiv:astro-ph/0306408.

[123] N. G. Lehtinen, P. W. Gorham, A. R. Jacobson and R. A. Roussel-Dupre, arXiv:astro-ph/0309656.

[124] K. Shinozaki *et al.*, Astrophys. J. **571** (2002) L117; K. Shinozaki *et al.*, *Prepared for 28th International Cosmic Ray Conferences (ICRC 2003), Tsukuba, Japan, 31 Jul - 7 Aug 2003*

[125] V.S.Berezinsky and A.Yu.Smirnov, Astrophysics and Space Science, **32**, 461 (1975); V. S. Berezinsky and G. T. Zatsepin, Soviet Physics - Uspekhi, **20**, 361 (1977).

[126] P. S. Coppi and F. A. Aharonian, Astrophys. J. **487**, L9 (1997) [astro-ph/9610176].

[127] E. Waxman and J. N. Bahcall, Phys. Rev. D **59**, 023002 (1999) [hep-ph/9807282]; J. N. Bahcall and E. Waxman, Phys. Rev. D **64**, 023002 (2001) [hep-ph/9902383].

[128] K. Mannheim, R. J. Protheroe and J. P. Rachen, Phys. Rev. D **63**, 023003 (2001) [astro-ph/9812398].

[129] For general information see http://wsgs02.lngs.infn.it:8000/macro/; see also M. Ambrosio *et al.* [MACRO Collaboration], astro-ph/0203181.

[130] S. Yoshida for the AGASA Collaboration, Proc. of 27th ICRC (Hamburg) **3**, 1142 (2001).

[131] R. M. Baltrusaitis *et al.*, Astrophys. J. **281**, L9 (1984) ; Phys. Rev. D **31**, 2192 (1985).

[132] see the thesis by K. Kim, http://www.cosmic-ray.org/thesis/kim/kimthesis.pdf.

[133] P. W. Gorham, K. M. Liewer and C. J. Naudet, astro-ph/9906504. . W. Gorham, K. M. Liewer, C. J. Naudet, D. P. Saltzberg and D. R. Williams, astro-ph/0102435,

[134] see, e.g., talk by U. Katz on HENA 2003 workshop, http://antares.in2p3.fr/antares/stolar/km3/program.htm.

[135] For general information see http://www.lal.in2p3.fr/recherche/nemo/.

[136] see S. Bottai and S. Giurgola, http://www-rccn.icrr.u-tokyo.ac.jp/icrc2003/PROCEEDINGS/PDF/279.pdf.

[137] C. Aramo, A. Insolia, A. Leonardi, G. Miele, L. Perrone, O. Pisanti and D. V. Semikoz, Astropart. Phys. **23**, 65 (2005) [arXiv:astro-ph/0407638].

[138] Z. Fodor, S. D. Katz, A. Ringwald and H. Tu, JCAP **0311**, 015 (2003) [arXiv:hep-ph/0309171].

[139] N. Hayashida *et al.*, Phys. Rev. Lett. **73**, 3491 (1994).

[140] L. Gonzales-Mestres, Nucl. Phys. B (Proc.Suppl.) **48**, 131 (1996); S. Coleman and S.L. Glashow, Phys. Rev. **D 59**, 116008 (1999); R. Aloisio, P. Blasi, P. Ghia, and A. Grillo, Phys. Rev. D **62**, 053010 (2000) [arXiv:astro-ph/0001258].

[141] M. Ahlers, A. Ringwald and H. Tu, Astropart. Phys. **24**, 438 (2006) [arXiv:astro-ph/0506698].

[142] G.R. Farrar, Phys. Rev. Lett. **76**, 4111 (1996). [arXive:hep-ph/9603271].

[143] D. J. Chung, G. R. Farrar and E. W. Kolb, Phys. Rev. D **57**, 4606 (1998) [arXiv:astro-ph/9707036]. See also S. Balberg, G. R. Farrar and T. Piran, Astrophys. J. **548**, L179 (2001) [arXiv:astro-ph/0010112].

[144] J. Adams *et al.* [KTeV Collaboration], Phys. Rev. Lett. **79**, 4083 (1997) [arXiv:hep-ex/9709028]; V. Fanti *et al.* [NA48 Collaboration], Phys. Lett. **B446**, 117 (1999); A. Alavi-Harati *et al.* [KTeV Collaboration], Phys. Rev. Lett. **83**, 2128 (1999) [arXiv:hep-ex/9903048].

[145] I.F. Albuquerque *et al.* [E761 Collaboration], Phys. Rev. Lett. **78**, 3252 (1997) [arXiv:hep-ex/9604002].

[146] V. Berezinsky, M. Kachelrieß, and S. Ostapchenko, Phys. Rev. D **65**, 083004 (2002) [arXiv:astro-ph/0109026].

[147] D. S. Gorbunov, G. G. Raffelt and D. V. Semikoz, Phys. Rev. D **64**, 096005 (2001) [arXiv:hep-ph/0103175].

[148] D.E. Groom *et al.* [Particle Data Group Collaboration], Eur. Phys. J. C **15** (2000) 1.

[149] E. Masso and R. Toldra, Phys. Rev. D **52** (1995) 1755 [hep-ph/9503293]. E. Masso and R. Toldra, Phys. Rev. D **55** (1997) 7967 [hep-ph/9702275].

[150] D.S. Gorbunov, hep-ph/0007325.

[151] G.G. Raffelt, "Stars as laboratories for fundamental physics: The astrophysics of neutrinos, axions, and other weakly interacting particles," *Chicago, USA: Univ. Pr. (1996) 664 p.*

[152] N. Rubin, M. Phil. Thesis, Cavendish Laboratory, University of Cambridge, 1999, http://www.stanford.edu/ nrubin/Thesis.ps Z. Fodor and S. D. Katz, Phys. Rev. Lett. **86**, 3224 (2001) [arXiv:hep-ph/0008204]. S. Sarkar and R. Toldra, Nucl. Phys. B **621**, 495 (2002) [hep-ph/0108098]. C. Barbot and M. Drees, Phys. Lett. B **533**, 107 (2002) [arXiv:hep-ph/0202072]; R. Aloisio, V. Berezinsky and M. Kachelriess, arXiv:hep-ph/0307279; C. Barbot and M. Drees, arXiv:hep-ph/0211406.

[153] Yu. L. Dokshitzer, V. A. Khoze, A. H. Mueller, and S. I. Troyan, *Basics of perturbative QCD* (Editions Frontiers, Saclay, 1991); R. K. Ellis, W. J. Stirling, and B. R. Webber, *QCD and Collider Physics* (Cambridge Univ. Press, Cambridge, England, 1996); V. A. Khoze and W. Ochs, Int. J. Mod. Phys. A12 (1997) 2949.

[154] V. Berezinsky, M. Kachelrieß and A. Vilenkin, Phys. Rev. Lett. **79**, 4302 (1997) [astro-ph/9708217].

[155] V. A. Kuzmin and V. A. Rubakov, Phys. Atom. Nucl. **61**, 1028 (1998) [Yad. Fiz. **61**, 1122 (1998)] [astro-ph/9709187].

[156] V. Kuzmin and I. Tkachev, Phys. Rev. D **59**, 123006 (1999) [hep-ph/9809547]; D. J. Chung, E. W. Kolb and A. Riotto, Phys. Rev. D **60**, 063504 (1999) [hep-ph/9809453].

[157] P. Blasi, R. Dick and E. W. Kolb, Astropart. Phys. **18**, 57 (2002) [astro-ph/0105232].

[158] S. L. Dubovsky and P. G. Tinyakov, JETP Lett. **68**, 107 (1998) [hep-ph/9802382].

[159] M. M. Winn, J. Ulrichs, L. S. Peak, C. B. Mccusker and L. Horton, J. Phys. G **12**, 653 (1986); see also the complete catalogue of SUGAR data in "Catalogue of highest energy cosmic rays No. 2", ed. WDC-C2 for Cosmic Rays (1986).

[160] A. Benson, A. W. Wolfendale and A. Smialkowski, Astropart. Phys. **10**, 313 (1999).

[161] L. A. Anchordoqui, C. Hojvat, T. P. McCauley, T. C. Paul, S. Reucroft, J. D. Swain and A. Widom, astro-ph/0305158.

[162] M. Kachelriess and D. V. Semikoz, arXiv:astro-ph/0306282;

[163] H. B. Kim and P. Tinyakov, arXiv:astro-ph/0306413.

[164] T. J. Weiler, Phys. Rev. Lett. **49**, 234 (1982). Astrophys. J. **285**, 495 (1984).

[165] T. J. Weiler Astropart. Phys. **11**, 303 (1999) [hep-ph/9710431]. D. Fargion, B. Mele and A. Salis, rays," Astrophys. J. **517**, 725 (1999) [astro-ph/9710029].

[166] S. Yoshida, G. Sigl and S. j. Lee, Phys. Rev. Lett. **81**, 5505 (1998) [hep-ph/9808324].

[167] S. Singh and C. P. Ma, Phys. Rev. D **67**, 023506 (2003) [arXiv:astro-ph/0208419].

[168] D. S. Gorbunov, P. G. Tinyakov and S. V. Troitsky, Astropart. Phys. **18**, 463 (2003) [arXiv:astro-ph/0206385].

[169] Z. Fodor, S. D. Katz and A. Ringwald, Phys. Rev. Lett. **88**, 171101 (2002) [hep-ph/0105064]; hep-ph/0105336; hep-ph/0203198; A. Ringwald, hep-ph/0111112.

[170] S. Hannestad, JCAP **0305**, 004 (2003) [arXiv:astro-ph/0303076].

[171] see, e.g., M. Maltoni, T. Schwetz, M. A. Tortola and J. W. Valle, arXiv:hep-ph/0309130.

[172] G. Gelmini and A. Kusenko, Phys. Rev. Lett. **84**, 1378 (2000) [arXiv:hep-ph/9908276].

[173] V. Berezinsky, M. Kachelriess and S. Ostapchenko, Phys. Rev. Lett. **89**, 171802 (2002) [arXiv:hep-ph/0205218].

[174] P. W. Gorham, C. L. Hebert, K. M. Liewer, C. J. Naudet, D. Saltzberg and D. Williams, Phys. Rev. Lett. **93**, 041101 (2004) [arXiv:astro-ph/0310232].